Journal Pre-proof

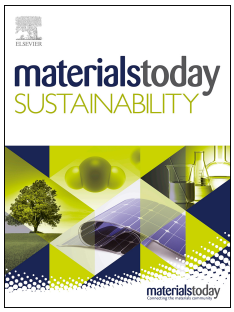

Enhancing Latent Heat Storage: Impact of Geometric Modifications, S-shaped enclosure Walls, and L-shaped fins

Houssam Eddine Abdellatif, Shan Ali Khan, Nahid Fatima, M.A. Aljohani, Adeel Arshad, Ahmed Belaadi, Abdullah Alhushaybari

PII: S2589-2347(25)00043-0

DOI: https://doi.org/10.1016/j.mtsust.2025.101114

Reference: MTSUST 101114

To appear in: *Materials Today Sustainability*

Received Date: 17 January 2025

Revised Date: 13 March 2025

Accepted Date: 5 April 2025

Please cite this article as: H.E. Abdellatif, S.A. Khan, N. Fatima, M.A Aljohani, A. Arshad, A. Belaadi, A. Alhushaybari, Enhancing Latent Heat Storage: Impact of Geometric Modifications, S-shaped enclosure Walls, and L-shaped fins, *Materials Today Sustainability*, https://doi.org/10.1016/j.mtsust.2025.101114.

Enhancing Latent Heat Storage: Impact of Geometric Modifications, S-shaped enclosure Walls, and L-shaped fins

Houssam Eddine Abdellatif[1, 2], Shan Ali Khan[3,*], Nahid Fatima[4], M.A.Aljohani[5], Adeel Arshad[6], Ahmed Belaadi[1], Abdullah Alhushaybari[7]

1. *Département de Génie Mécanique, Faculté de Technologie, Université 20 Août 1955-Skikda, Algérie.*
2. *Laboratoire LGMM, Université 20 Août 1955- Skikda, Algérie.*
3. *Department of Mathematics, Government College University Faisalabad, 38000, Pakistan*
4. *Department of Mathematics and Sciences, Prince Sultan University, Riyadh 11586, Saudi Arabia*
5. *Department of Mathematics and Statistics, College of Science, Taibah University, Yanbu, Saudi Arabia*
6. *Department of Mechatronics and Biomedical Engineering, School of Engineering and Technology, Aston University, Birmingham B4 7ET, United Kingdom.*
7. *Department of Mathematics, College of Science, Taif University, P.O. Box 11099, Taif 21944, Saudi Arabia*

Corresponding authors: shanalikhan@stu.xjtu.edu.cn (Shan Ali Khan)

Abstract

This study explores the thermal performance and phase change behavior of five thermal energy storage (TES) models with varied geometric and design parameters, aiming to enhance heat transfer and storage efficiency.The impact of an innovative S-shaped heat source wall configuration and L-shaped fins on phase change dynamics was examined through numerical simulations, presenting a novel approach to enhancing TES system designs. Temperature distribution, transient PCM temperature, velocity fields, and liquid fraction evolution were analyzed to evaluate melting time, energy storage density (SE_m), mean power (P_m), and total heat storage capacity. The findings indicate that geometric enhancements and fin configurations significantly influence phase change performance. Model 01 exhibited the longest melting time of 11,040 s, whereas Model 05, with enhanced thinner (0.3 mm) and longer (112.3 mm) fins, achieved the shortest melting time of 2,720 s, reducing melting time by 75.36%. Model 05 also demonstrated the highest $SE_m$of 274.12 kJ/kg and Pm of 67.72 W, highlighting its superior thermal storage efficiency. These results

emphasize the crucial role of fin geometry and enclosure profiles in improving TES system performance.

Keywords: *Thermal Energy Storage (TES), Phase Change Materials (PCM), Melting Time Reduction, Energy Storage Density (SE_m).*

Nomenclature		**Greek symbols**	
A_m	The mushy zone (kg/s m^3)	β	Thermal expansion coefficient (1/K)
C_p	Thermal capacity(J/K)	λ	Latent heat capacity (J/kg)
D_h	Hydraulic diameter(mm)	μ_{PCM}	Dynamic viscosity of PCM (Pa·s)
g	Gravity(m/s^2)	ε	Constant
H	Enthalpy of the PCM(J/kg.K)	ρ_{PCM}	PCM Density (kg/m^3)
h_s	Sensible enthalpy (J/kg.K)	γ Lquidfraction of PCM (%)	
m_{PCM}PCM mass (kg)			
P_mMean power (W)		**Abbreviations**	
q''	Heat flux (W/m^2)	CFD	Computational Fluid Dynamic
QThermal energy storage (KJ)			
SE_mEnergy storage density (KJ/kg)		LHTES	Latent Heat Thermal Energy Storage
t_mMelting time (s)		PCM	Phase Change Material
$Tref$	Reference temperature (K)	SIMPLE	Semi-Implicit Method for Pressure
		TES	Thermal Energy Storage

Highlights

- Developed enhanced TES models with L-shaped fins and an S-shaped heat source.
- Examined the impact of geometric modifications on melting time.
- Enhanced L-shaped fins inside the enclosures to achieve significant improvements.
- Demonstrated increased energy storage density and improved thermal performance.

1. Introduction

Energy consumption has dramatically increased due to population growth, urbanization, fast industrialization, and technological improvements. Fossil fuels continue to be the dominant

source of energy for many sectors, which accelerates climate change and raises atmospheric concentrations of greenhouse gases. On the other hand, because of their environmental friendliness, renewable energy sources like geothermal, solar, wind, hydropower, and biofuels have drawn more attention. Solar energy stands out among these as a sustainable and clean alternative that doesn't pollute the environment. Furthermore, solar thermal and photovoltaic (PV) technologies can be utilized to capture sun energy and convert it into electrical power [1]. Renewable energy, particularly solar energy, has received more attention in recent years since it is clean and widely available [2]. However, the transformation and consumption of renewable energy frequently encounter temporal and spatial incompatibilities [3]. To solve this issue, latent heat thermal energy storage (LHTES) technology [4] has emerged as a critical solution for bridging the energy supply and demand gap.

The depletion of fossil resources and environmental deterioration have become important issues, impeding long-term global economic and social progress. Among the urgent concerns confronting the globe today are rising energy consumption and ongoing environmental degradation. As a result, renewable energy sources such as solar and wind power have received substantial attention as emerging energy technologies. Solar energy, in particular, stands out as one of the mainly capable renewable sources, extensively used across a variety of industries due to its numerous benefits, which include cheap operational costs, zero emissions, ease of access, and abundant reserves. Solar collectors (SCs) are a simple and cost-effective way to exchange solar irradiance into thermal energy by capturing heat from sunlight [5]. Flat plate solar collectors are especially helpful since they are simple to operate and cost less than other forms of solar collectors. Solar collectors are divided into two types based on the working fluid they use: solar air collectors (SACs) and solar water collectors (SWCs). SACs are available in a variety of configurations and are widely used in building-integrated air heating and drying applications. However, the usage of air, which has a lower heat transfer coefficient than water, and the absence of inherent heat storage capabilities are significant limits of SACs [6]. To address these drawbacks, heat storage systems have been integrated into SACs in recent years. These advancements have enhanced the functionality of SACs, making them more suitable for heating and agricultural drying, especially during cloudy weather and nighttime conditions [7].

Thermal energy storage (TES) systems can be smoothly linked with renewable energy sources to satisfy crucial energy needs. In today's world, energy has become so important that its scarcity creates substantial dangers, such as probable industrial and power plant shutdowns, transit disruptions, limited fuel availability for vehicles, winter school closures,

and grounded aircraft. The mastering of fire was a watershed moment in human evolution, and advances in energy storage continue to influence current civilization. Recently, a variety of phase change materials (PCMs) have been developed for use in latent heat storage systems [8], [9], [10], [11], [12], [13]. Thermal energy storage (TES) methods include a wide range of temperature regimes, including low, moderate, high, and ultra-low temperatures. This research investigates the establishment of important criteria, functional characteristics, and an appropriate model for TES systems. The utilize of phase change materials (PCMs) in latent heat storage is highlighted, with a particular emphasis on high-temperature applications where inorganic materials show significant potential. Given humans' enormous thermal energy consumption, developments in thermal energy management systems based on TES can deliver major social advantages. Thermal energy storage (TES) systems were thoroughly examined by Alva et al. [14]. Sharma et al. [15] talked about different thermal energy storage techniques and their uses, while Sarbu and Sebarchievici[16] gave a thorough study of TES technologies. Ben Khedher et al. [17] optimized PCM melting in a double-pipe heat exchanger using framed structures, achieving 55% faster melting and 115% higher storage rate.In another study [18], they optimized circular Y-shaped fins in a double-tube heat exchanger with PCM, achieving a 22% reduction in solidification time and a 26% increase in discharging rate compared to straight fins. Sardari et al. [19] investigated PCM melting in a vertical heat storage system with copper metal foam, achieving an 85% reduction in melting time compared to PCM alone.

Over the last three decades, PCMs for thermal energy storage have received substantial research due to their high thermal energy density per unit volume or mass, as well as their adaptability across a wide temperature range in a variety of technical applications. Recent studies have identified key challenges in phase change modeling, including convective false diffusion, asymmetrical solid-liquid interfaces, and equilibrium state correlations in enthalpy-porosity methods [20]. These factors must be carefully considered to enhance numerical accuracy in PCM-based thermal energy storage systems. PCM-based TES is critical for closing the energy supply-demand gap and increasing the effectiveness of solar energy systems. PCMs are widely used in various scientific and technological fields, including thermal energy storage in building structures [21], [22], [23], [24], construction systems such as domestic hot water, cooling, TES systems [25], [26], and heating mechanisms [27], electronic devices [28], [29], drying systems [30], waste heat recovery [31], cooling and cold preservation technologies [32], and electrical and electronic equipment [33]. PCMs have numerous advantages, including practically constant thermal energy throughout phase

transitions and a high energy storage density, which ensures increased reliability and efficiency in various applications. The thermal performance of a finned PCM cavity was scrutinized experimentally and computationally by Hosseinizadeh et al. [34]. The impacts of fin height, thickness, and number were the main focus of their analysis. The findings showed that while fin thickness did not affect thermal efficiency, increasing the number or height of fins enhanced heat transfer and shortened melting time. Sadeghi et al. [35] investigated the impact of charging and discharging processes on multilayer PCM topologies in heat exchangers. According to their research, a three-layer PCM system can save up to 41.67% in energy. By contrasting fin-equipped and fin-less designs, Dhaidan et al. [36]scrutinized the melting process of PCM in heat exchangers. Their findings showed that, in comparison to fins without perforations, fins with perforations performed better thermally.Abed et al. [37]enhanced PCM melting in a triplex-tube system using arc-shaped fins, achieving 93.1% faster melting and 50.4% shorter melting time compared to no fins.Dhaidan et al. [38]introduced the significance of geometrical elements like aspect ratio and eccentricity in circular cavities in a different study on PCM melting and convection in containers of dissimilar shapes. They found that conduction dominated heat transfer at first, but as the molten liquid layer grew, convection took over. To investigate the mixed convection of PCM in a square cavity impacted by a spinning cylinder, Selimefendigil et al. [39] used a numerical simulation. They examined how the cylinder's size, vertical position, and angular velocity affected the process of heat transmission. According to the findings, the average Nusselt number rose by 22.50% from the stationary condition at an angular velocity of 7.5 rad/s.

Recent theoretical, computational, and experimental research have shown that solar thermal systems combined with PCMs are viable solutions for tackling issues related to low solar radiation and energy storage at night. Experimental studies of the thermal efficiency of a flat plate solar air collector (SAC) combined with PCM were carried out by El Khadraoui et al. [40]. In comparison to the SAC without PCM, the study discovered that the SAC with PCM provided better drying conditions, especially at night. Palacio et al. [41]investigated the impact of phase change material on solar air heater performance. They concluded that the performance of solar air heaters is boosted by using the phase change material. Recently many studies [42], [43], [44], [45] are carried out for solar thermal systems by using phase change material.

Despite extensive research on PCM-based TES systems, most studies have focused on conventional designs with limited geometric optimizations. This study introduces an

innovative TES model incorporating an S-shaped heat source wall and L-shaped fins to enhance phase change behavior. Through numerical simulations, we systematically analyze the impact of fin geometry and heat source configurations on thermal performance. The key contributions of this study include (i) proposing a novel TES configuration that improves heat transfer efficiency, (ii) evaluating the impact of fin thickness, fin length, and heat source shape on melting time, energy storage density, and mean power, and (iii) demonstrating a significant reduction in melting time with enhanced fin designs. These findings offer valuable insights for designing high-efficiency TES systems suitable for renewable energy applications.

2. Model description

2.1. Physical domain description

This study investigates the thermal performance of rectangular PCM containers designed for thermal energy storage. The configurations vary based on wall geometry and fin integration to enhance heat transfer efficiency.

-Model 01 (Baseline Model): A simple rectangular container with dimensions L = 120 mm and W = 50 mm. The right wall serves as the heat source, maintained at 343.15K.

-Model 02 (S-Shaped Wall): The right wall (heat source) is reshaped into a curved, S-shaped profile with a diameter of D = 60 mm, while keeping the heat source temperature at 343.15K. This modification increases the contact area between the heat source and PCM, promoting faster melting.

-Model 03 (S-Shaped Wall + L-Shaped Fins): L-shaped fins are attached to the curved heat source wall to enhance thermal performance. The fins have a small length of ω = 25 mm, a larger length of L = 50 mm, and a thickness of e = 1 mm. The added fins improve heat transfer by increasing the surface area exposed to the PCM.

-Model 04 (Extended Fins with Reduced Thickness): The fin configuration is further enhanced by extending the larger fin length to L = 90 mm and reducing the thickness to e = 0.5 mm. The fins have a small length of ω = 25 mm, enhancing heat dissipation and accelerating PCM melting.

-Model 05 (Enhanced Long and Thin Fins): The larger fin length is increased to L = 112.3 mm, while the thickness is further reduced to e = 0.3 mm. The fins have a small length of ω = 25 mm, achieving the highest melting efficiency due to a maximized heat transfer area.

The use of aluminum for both the L-shaped fins and the S-shaped heat source wall provides a cost-effective solution while ensuring favorable thermal properties. The S-shaped wall, with

its larger surface area compared to a traditional straight design, increases the heat transfer efficiency but also requires more aluminum, thus raising the cost. Similarly, the addition of L-shaped fins increases the surface area further, enhancing heat transfer but also contributing to a higher quantity of aluminum used. This added material, along with the precision machining and bending required for both the fins and the S-shaped wall, increases production costs. Although aluminum is relatively inexpensive, the need for specialized manufacturing techniques to achieve the necessary accuracy for these complex geometries leads to higher production and assembly costs. These factors should be considered for large-scale implementation in TES systems.

Figure 1 illustrates the physical domain of a rectangular enclosure (Model 01) and modified enclosure (Model 02), while **Figure 02** illustrates the 2D and 3D structure for case 02 and Models 03,04 and 05 (with fins). **Table 01** presents the dimension values for all Models.**Table 2** summarizes the thermophysical values of Lauric acid utilized in this study. These properties were essential for accurately modeling the phase change behavior and thermal performance of the PCM under various configurations.

The S-shaped heat source wall increases the heat transfer surface, enhancing PCM melting, while the L-shaped fins further improve thermal propagation. This design is crucial for TES systems in renewable energy applications, enhancing heat storage, reducing charging time, and improving energy efficiency.

Table 1. Dimensions of all enclosure models detailed specifications and design parameters.

	D (mm)	L(mm)	W(mm)	ℓ(mm)	ω(mm)	e(mm)
Model 01	-	120	50	-	50	-
Model 02	60	120	50	-	50	-
Model 03	60	120	50	50	50	1
Model 04	60	120	50	90	50	0.5
Model 05	60	120	50	112.3	50	0.3

Table 2. Thermophysical properties for Lauric acid [46].

Property	values
Density (kg/m^3)	940(s)/885(l)
Specific heat capacity (J/Kg. K)	2180(s)/2390(l)

Thermal conductivity (W/m. K)	0.16(s)/0.14(l)
Dynamic viscosity (Kg/m.s)	0.008
Latent heat (J/Kg)	187210(l)
Temperature (K)	316.65(s)/321.35(l)
Thermal expansion coefficient (1/K)	0.0008

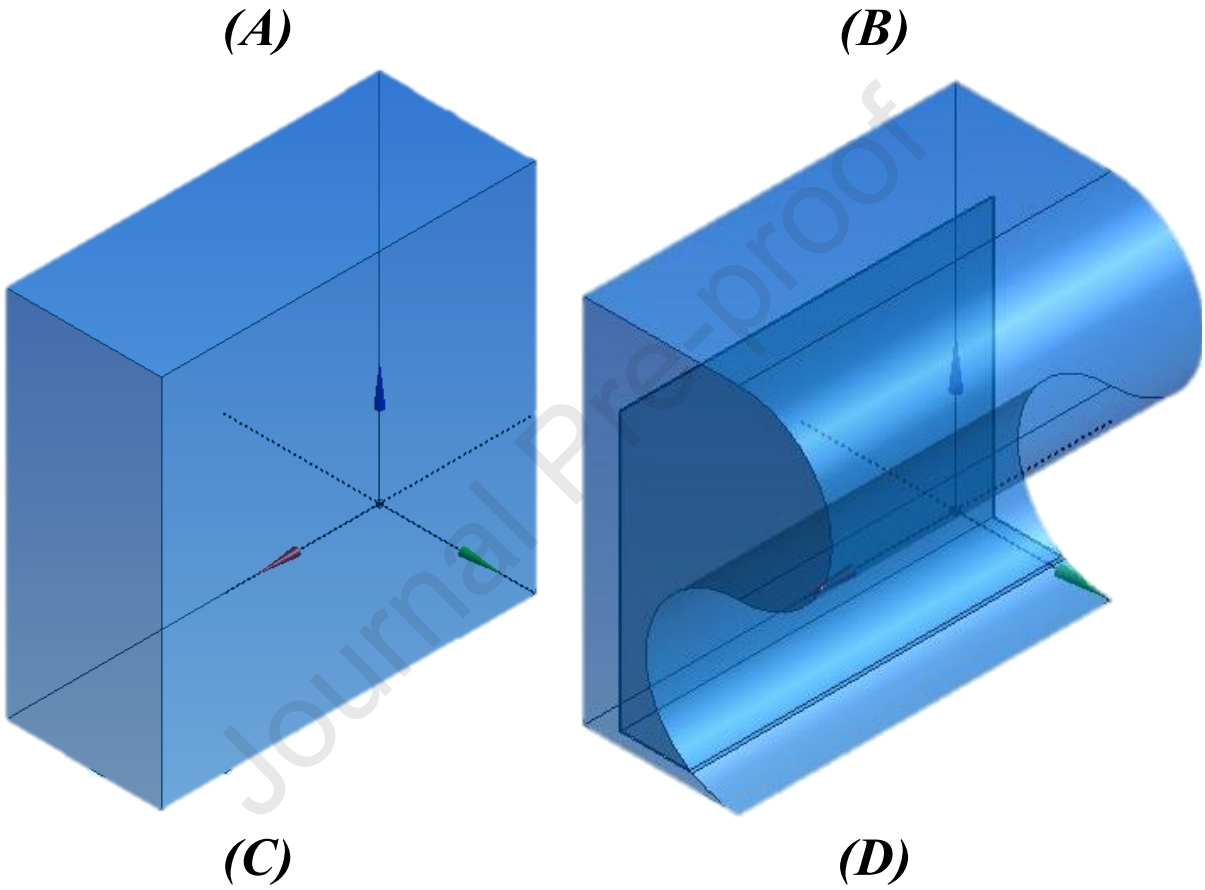

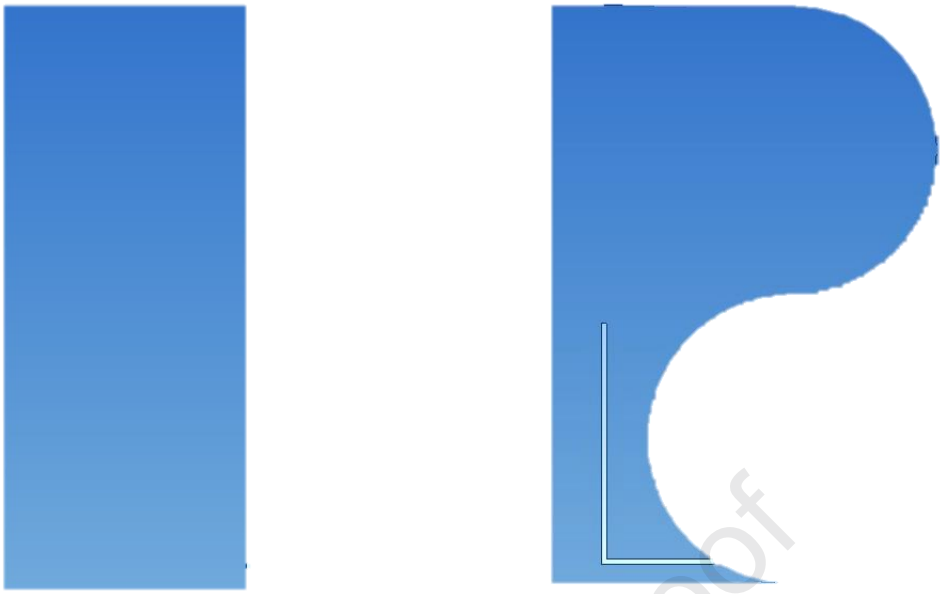

Fig 1. Geometric Designs of the PCM Enclosures: (A)- 3D PCM Rectangular Enclosure, (B)- 3D PCM Enclosure with S-shaped profile,(C)- 2D PCM Rectangular Enclosure with PCM, (D)- 2D PCM Enclosure with S-Shaped Profile.

3D structure	2D structure
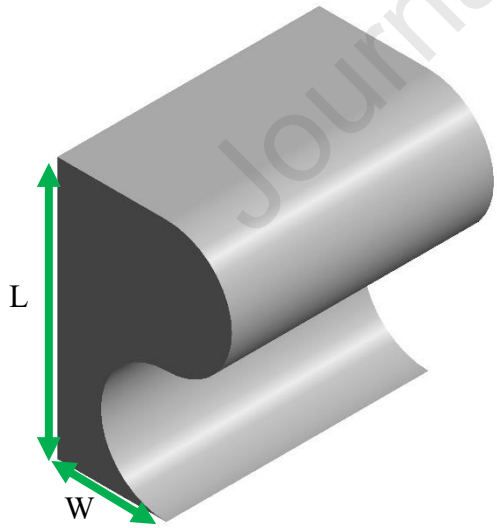	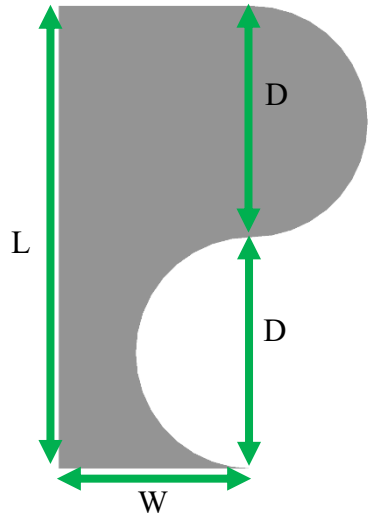

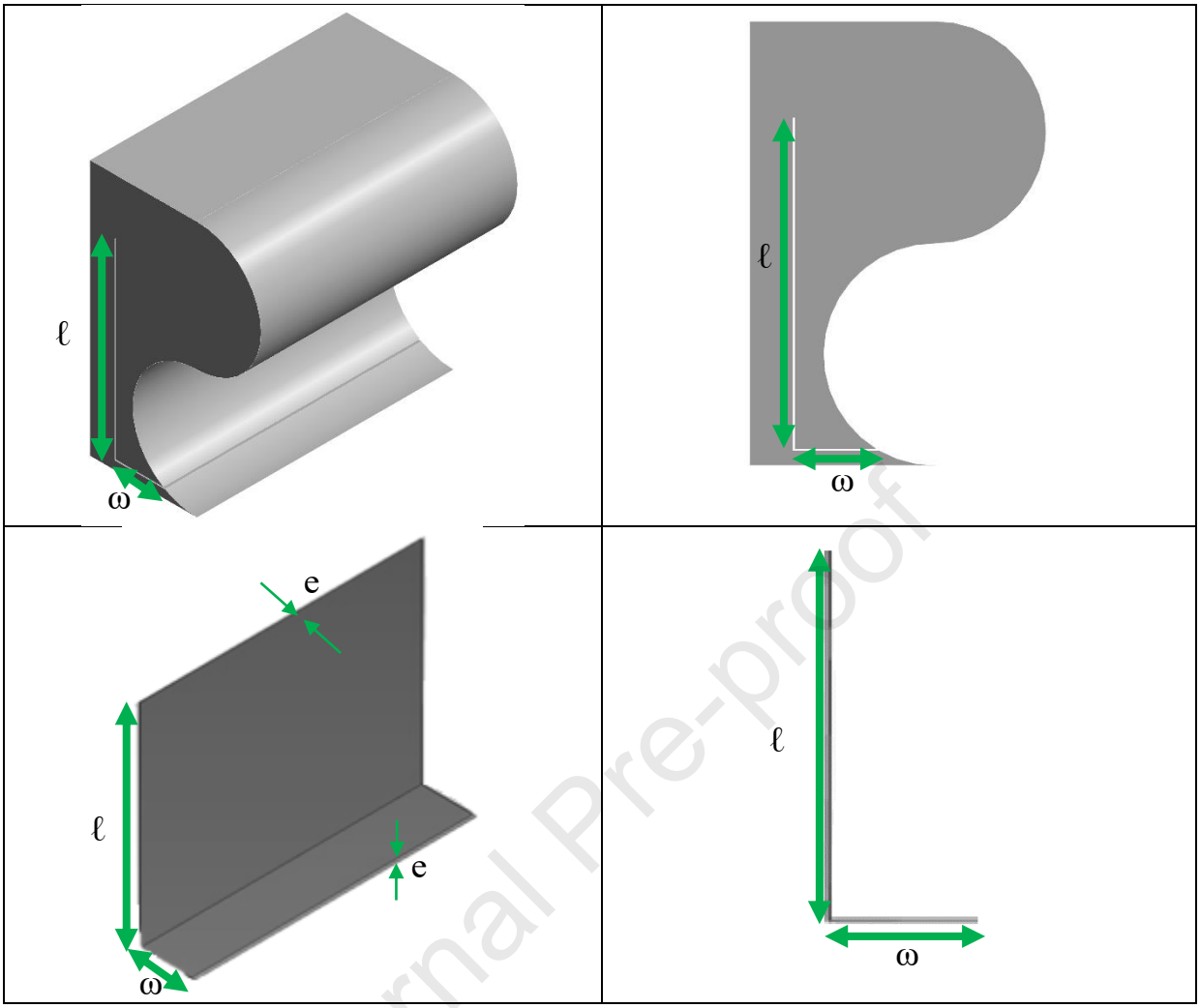

Fig 2. Dimensions of the S-Shaped Profile Enclosure and Fins.

2.2. Assumptions

The designed numerical model, which governs the melting of phase change material across a rectangular domain, is on the following fundamental assumptions:

- The two-dimensional, unsteady flow model is developed during the melting process, as supported by Biao Ye et al.[47], who demonstrated that 2D simulations can effectively replace 3D ones due to significantly reduced computational costs while maintaining accuracy.
- The liquid PCM flow is considered to be laminar, incompressible, and Newtonian.
- The Boussinesq model is employed to illustrate the density change and how it affects natural convection.
- The temperature-independent thermophysical properties of phase change used.

2.2. Mathematical model

The mathematical model for the current model under above discussed assumptions is defined as[48]:

Model for mass preservation:

$$\frac{\partial \rho_{pcm}}{\partial t} + \vec{\nabla}.\rho_{pcm}\vec{V} = 0. \tag{1}$$

Model for momentum preservation as per x-direction:

$$\rho_{pcm}\left[\frac{\partial u_1}{\partial t} + \left(\vec{V}.\vec{\nabla}\right)u_1\right] = -\frac{\partial p}{\partial x} + \mu_{pcm}\nabla^2 u_1 + S_x. \tag{2}$$

Model for momentum preservation as per y-direction:

$$\rho_{pcm}\left[\frac{\partial v_1}{\partial t} + \left(\vec{V}.\vec{\nabla}\right)v_1\right] = -\frac{\partial p}{\partial x} + \mu_{pcm}\nabla^2 v_1 + \left(\rho\beta\right)_{pcm} g\left(T - T_m\right) + + S_x. \tag{3}$$

Model for energy conservation:

$$\frac{\partial\left(\rho_{pcm}H\right)}{\partial t} + \nabla.\left(\rho_{pcm}\vec{V}H\right) = \nabla.\left(k_{pcm}\nabla T\right) \tag{4}$$

The Boussinesq hypothesis is addressed as:

$$\left(\rho - \rho_0\right)g = -\rho_0\beta\left(T - T_0\right). \tag{5}$$

here $\vec{V} \rightarrow$ indicates the velocity vector (velocity component in *x* and *y* directions), $t \rightarrow$ is the time, $\rho_{pcm} \rightarrow$ represent the density of phase change material, $\mu_{pcm} \rightarrow$ signify the dynamic viscosity of PCM, $p \rightarrow$ is the pressure, $g \rightarrow$ be the gravitational acceleration, and ($H \rightarrow$) denotes the material enthalpy. In the mushy zone, the source terms can be defined as[49]:

$$\vec{S} = A_{mushy}\left(\frac{1-\gamma}{\gamma^3 - \varepsilon}\right)\vec{V}. \tag{6}$$

Here, the melting nature of the phase change material is imitated by the mushy zone constant, A_{mushy}, $\gamma \rightarrow$ be the liquid fraction and $\varepsilon \rightarrow$ indicate the constant with a value of 0.001.

Furthermore, the specific enthalpy (H) is described as the sum of latent enthalpy (ΔH) and sensible enthalpy (h_s).

$$H = h_s + \Delta H. \tag{7}$$

were

$$h_s = h_{ref} + \int_{T_{ref}}^{T} C_p dT. \tag{8}$$

Here $h_{ref} \rightarrow$ indicate the reference enthalpy and ($T_{ref} \rightarrow$) is the reference temperature.

The content of latent heat content can be expressed as,

$$\Delta H = \gamma\lambda \tag{9}$$

The liquid fraction (γ) can be addressed as[49]:

$$\gamma = \frac{\Delta H}{\lambda}\begin{cases} 0, & \mathrm{T} < \mathrm{T}_s \\ \dfrac{T - T_s}{T_l - T_s}, & T_s \le T \le T_l \\ 1 & T \ge T_l \end{cases} \tag{10}$$

were $T_s \rightarrow$ indicate the solidus temperature and $T_l \rightarrow$ is liquidus temperature of phase change material.

The sensible heat, latent heat, and total heat of the thermal storage process are[50], [51]:

$$Q_{sensible} = mC_p\left(T_c - T_i\right) \tag{11}$$

$$Q_{latent} = m\lambda\gamma \tag{12}$$

$$Q_{total} = Q_{sensible} + Q_{latent} \tag{13}$$

2.3. Initial and boundary conditions

In the enclosure shown in **Figure 3**, one wall is maintained at a steady temperature of 70 °C (343.15 K), while the other three walls are thermally insulated to prevent heat exchange. The system is initially at a uniform temperature of 25 °C (298.15 K) throughout its domain.

The initial condition for the system is expressed as:

$$T(x, y, t = 0) = T_{initial} = 298.15K \tag{14}$$

The boundary condition for the wall held at 70 °C (343.15 K) is given by:

$$T(x, y, t) = T_{Wall} = 343.15K \tag{15}$$

For the insulated walls, the no-heat-flux condition applies, ensuring no thermal energy transfer through these boundaries.

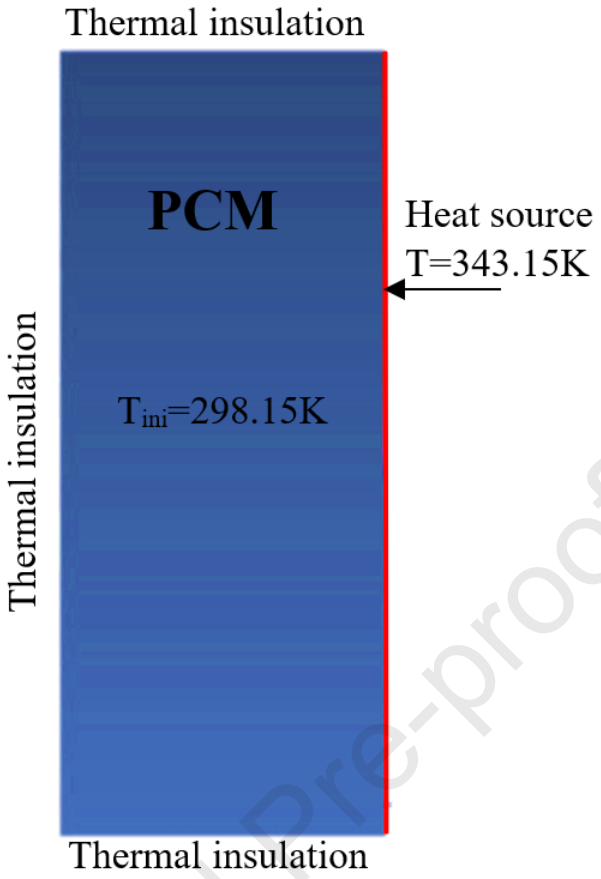

Fig 3. Boundary and initial conditions.

3. Numerical method and validation

3.1. Meshing and numerical process

The computational domain was discretized using a structured quadrilateral mesh, as shown in **Figure 4**, ensuring uniformity and computational efficiency. Simulations were performed using ANSYS Fluent 2024-R1 with double precision, employing a pressure-based transient solver and a laminar viscous model. Boundary conditions included no-slip walls, with three adiabatic walls and one wall maintained at a constant temperature. The materials used were phase change material (PCM) and aluminum (**Figure 5**). To enhance accuracy in capturing complex flow regions, a second-order upwind scheme was applied to the momentum equations, while the QUICK scheme was utilized for energy equations to model convective heat transfer. The SIMPLE algorithm coupled pressure and velocity in the momentum equations, with the PRESTO! (Pressure Staggering Option) scheme applied for pressure correction to ensure convergence and stability. Under-relaxation factors were set as follows: 0.3 for pressure, 0.7 for momentum, and 1 for energy, density, body forces, and liquid-

fraction update (**Figure 6**), ensuring stable convergence and accurate representation of physical phenomena throughout the simulation.

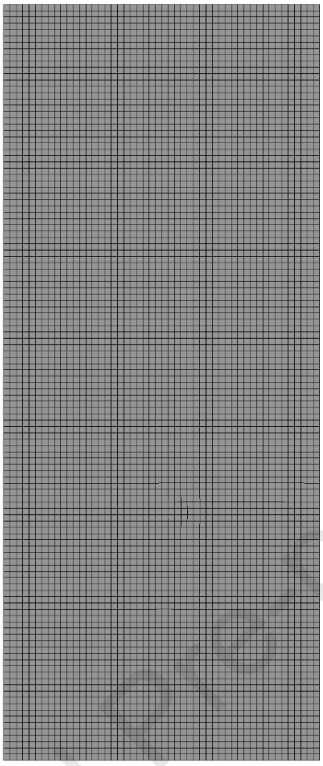

Fig 4. Mesh distribution in the computational domain.

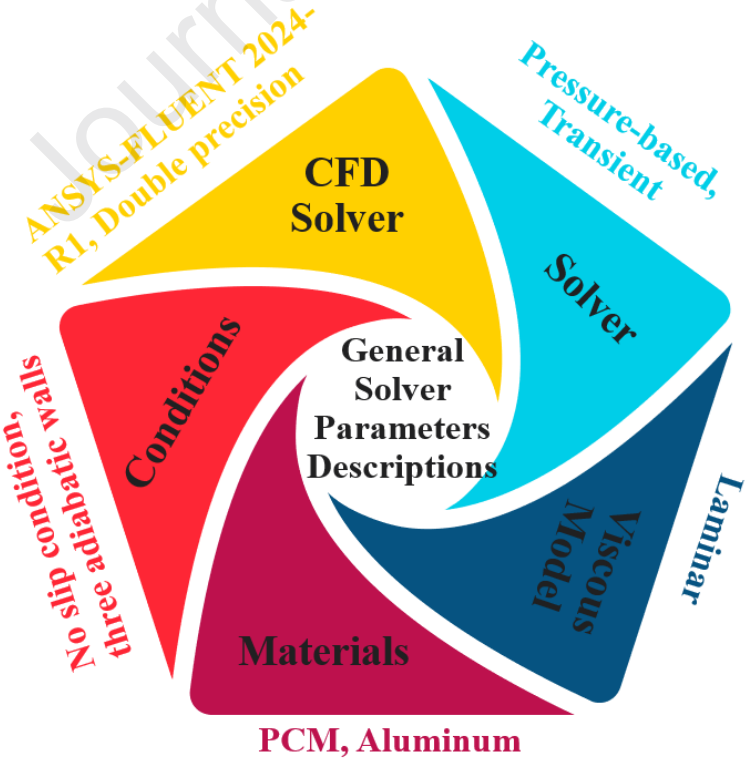

Fig 5. Solver Configuration for numerical solution process.

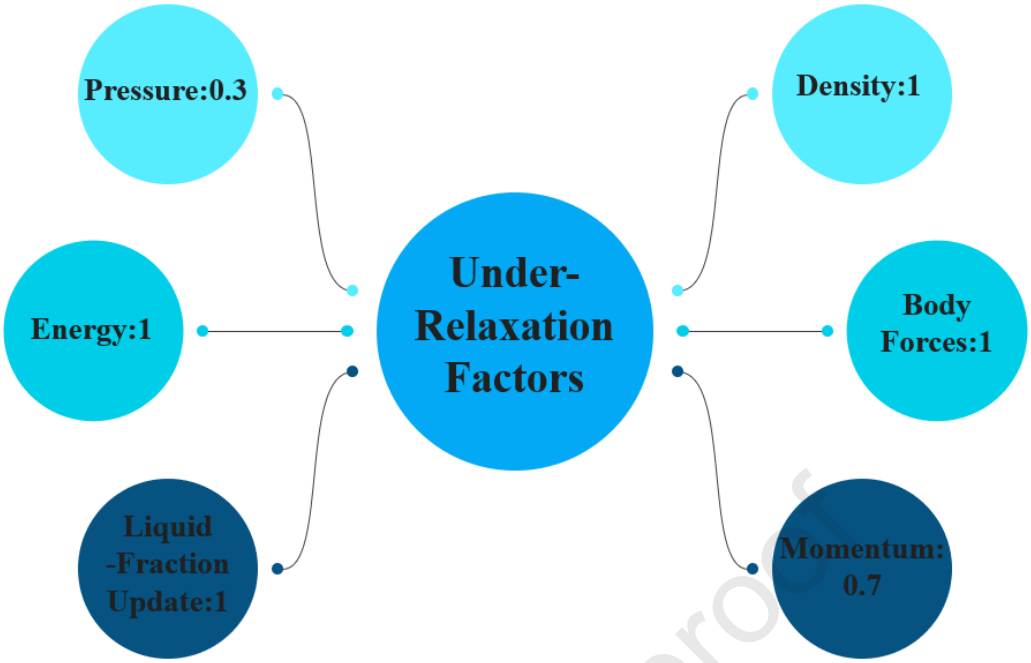

Fig 6. Under-Relaxation Factors for different parameters.

3.2. Time step independence study

A detailed analysis was conducted to evaluate the influence of the time step size on the accuracy and computational efficiency of the simulations. Using the selected mesh of 7,448 elements, simulations were performed with three dissimilar time steps: 0.2s, 0.5s, and 1s. The liquid fraction of the PCM was monitored as the key parameter to assess the effect of the time step size, as depicted in **Figure 7**. The analysis revealed negligible variations in the liquid fraction predictions across the tested time steps, confirming that the time step size did not significantly affect the simulation results. Consequently, a time step of 1 second was adopted, as it offered an optimal balance between computational cost and result accuracy for the current study.

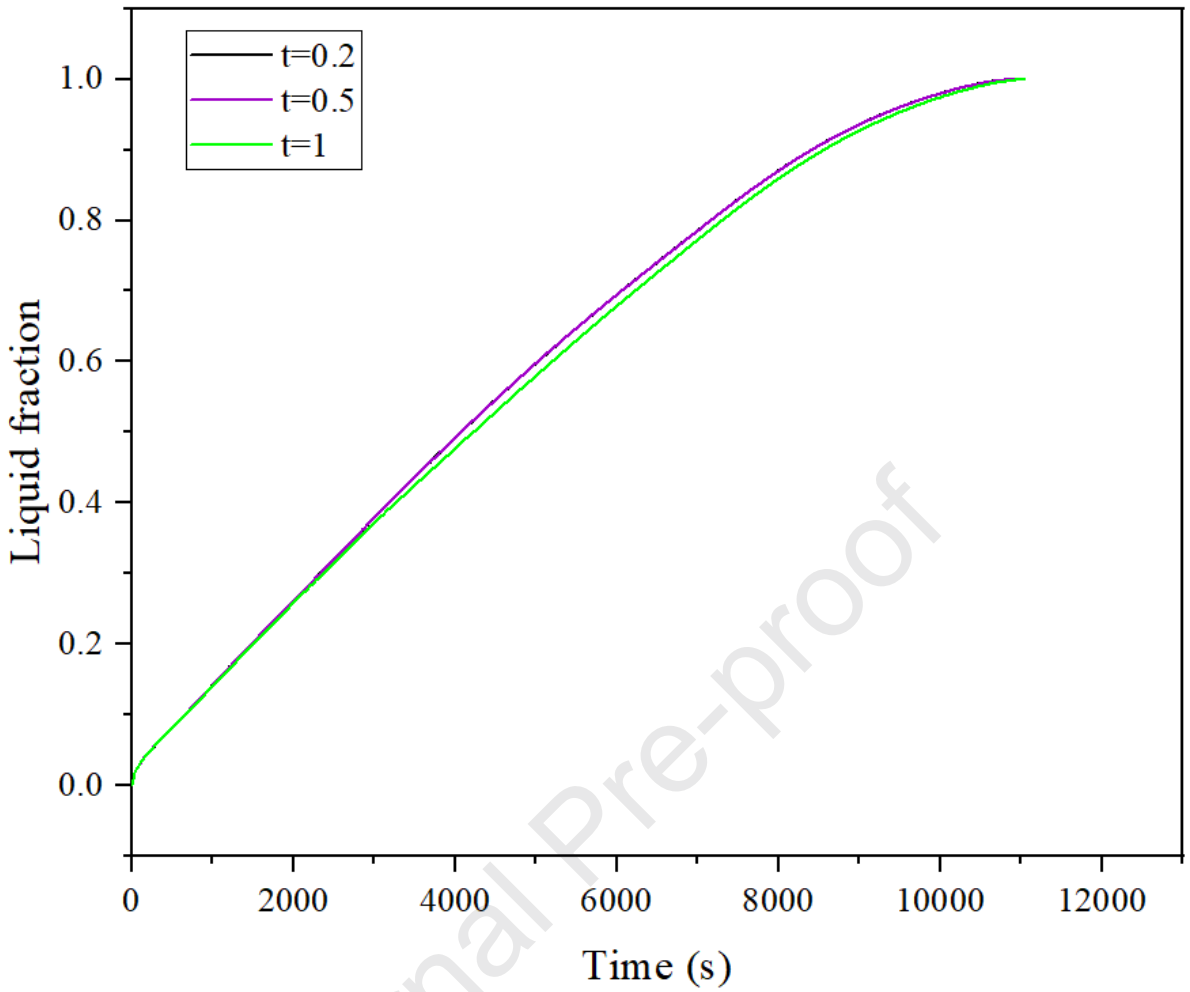

Fig 7. Time step independence analysis for numerical accuracy.

3.3. Model validation

Figure 8 compares the numerical predictions of the liquid fraction evolution and transient PCM temperature profiles with experimental data, revealing excellent agreement between the two. Minor deviations are observed, which can be attributed to uncertainties in experimental measurements and simplifications in the numerical model, such as material properties and boundary conditions. Despite these discrepancies, the relative error remains within an acceptable range, confirming the validity of the numerical approach for further parametric investigations. Additionally, previous studies on enthalpy-porosity modeling of phase change processes, particularly for pure gallium melting, have emphasized the importance of accurately defining interface-position errors and selecting appropriate numerical schemes to minimize discrepancies. These findings highlight the necessity of considering both global parameters (e.g., liquid fraction) and local parameters (e.g., interface position) to ensure robust validation of the numerical model[52].

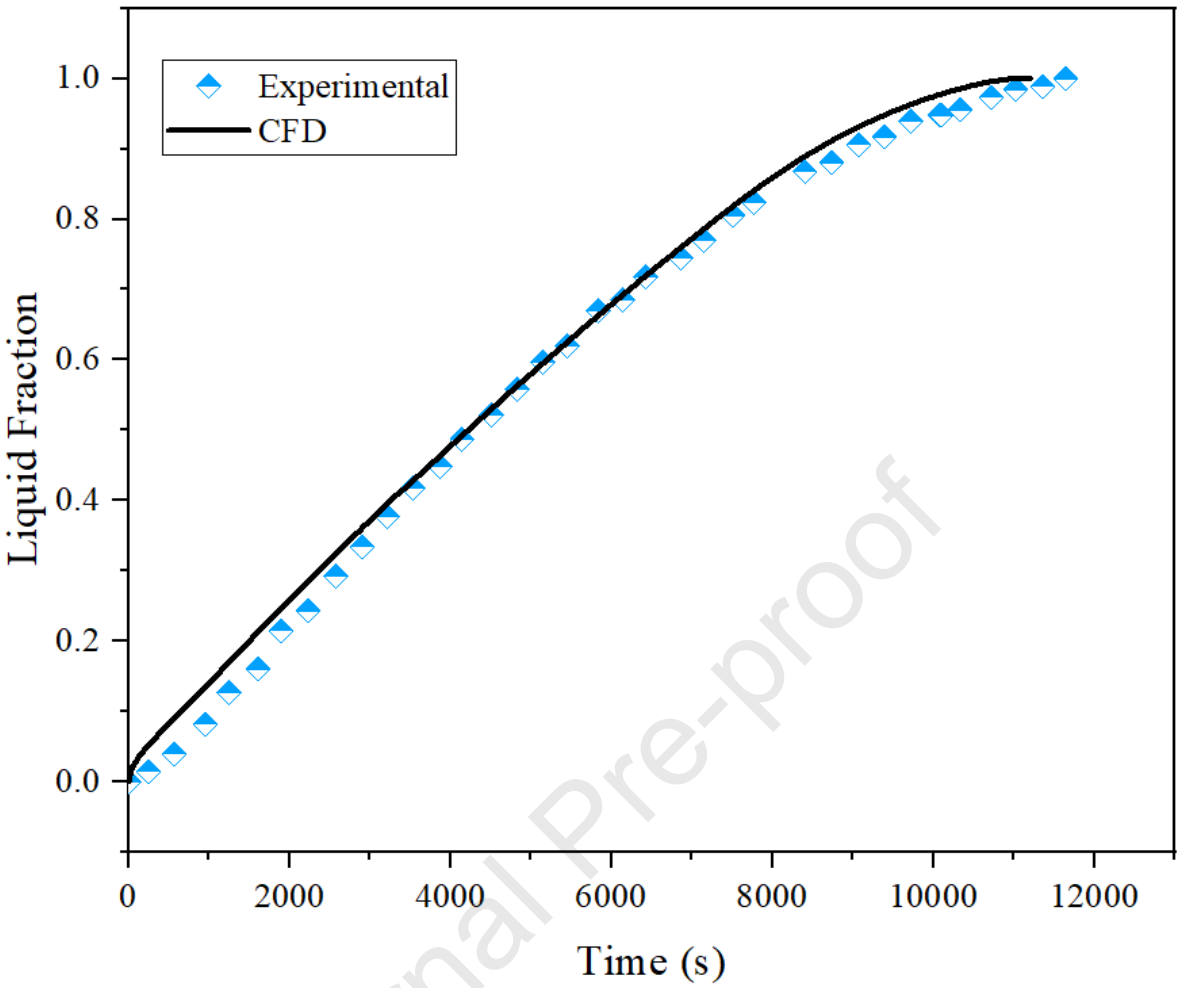

Fig 8. Liquid Fraction Variation: A Comparison with Kamkari et al. [53].

Mushy zone constant (A_m) is a crucial parameter in the momentum source term of the enthalpy-porosity technique for modeling convection-diffusion solid-liquid phase change[54].**Figure 9** illustrates the experimentally measured positions of the solid-liquid interface during the melting process within a vertically oriented enclosure at intervals of 10, 20, 30, 40, 60, and 80 minutes. The numerical simulation, incorporating a mushy zone constant of 5×10^5, was utilized to model the melting process at a wall temperature of 70 °C. The results closely match the experimental observations, as documented in [53], providing both melting profiles and liquid fraction distributions over time. The high level of consistency between the simulation and experimental data highlights the robustness and accuracy of the computational model in capturing the phase change dynamics within the system.

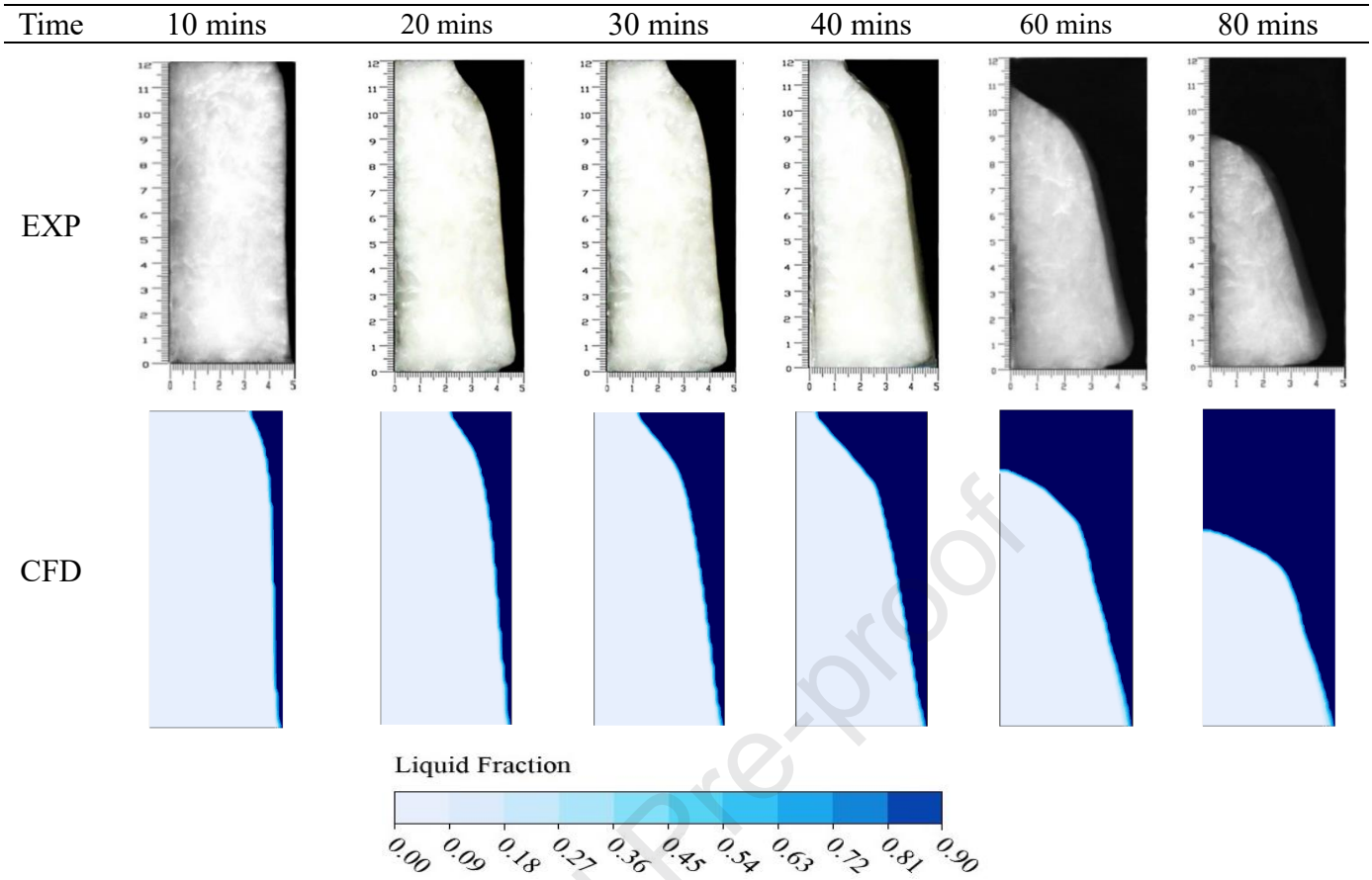

Fig 9. Temporal comparison of solid-liquid interface in experimental and simulated data.

4. Results and discussion

This section presents an in-depth analysis of the thermal performance of rectangular PCM containers with various design modifications, focusing on melting dynamics, heat transfer efficiency, and velocity fields. By examining the impact of reshaped heat source profiles and the incorporation of fins with varying dimensions, the study aims to identify configurations that enhance PCM melting efficiency. The results provide valuable insights into the influence of geometrical enhancements on thermal energy storage performance, guiding future design improvements.

4.1. Thermal Performance Analysis

4.1.1. Temperature Contours

The temperature contours in **Figure 10** depictthe heat transfer progression and melting behavior of PCM across five different configurations at intervals of 200s, 800s, 1600s, 2400s, and 2720s. In Model 01, the rectangular container exhibits a uniform PCM distribution. This configuration results in slower melting at the bottom due to the large PCM mass and the

natural convection heat transfer which leads the heat to the enclosure top. Heat is initially distributed through conduction near the heated wall, followed by convection, which moves the heat upward, melting the PCM at the top. This phenomenon occurs because, as the PCM melts, its density decreases, making the molten PCM lighter, which causes it to rise to the top while the denser, cooler PCM remains at the bottom. Consequently, the heat transfer becomes more dominant in the upper regions, leading to a delayed melting process in the lower sections.

In contrast, Model 02 introduces an S-shaped curved profile, which fundamentally alters the PCM distribution. This design reduces the PCM quantity at the bottom and redistributes it toward the top of the enclosure. Additionally, the S-shaped profile increases the heat source surface, enhancing the heat transfer process. Consequently, when heat enters through the right wall, it first propagates by conduction and then ascends due to natural convection. This upward heat flow encounters a greater PCM quantity at the top, promoting faster melting in the upper region. Furthermore, the reduced PCM quantity at the bottom requires less heat for melting, preventing excessive heat accumulation in the lower region and resulting in a more efficient and uniform heat transfer pattern throughout the enclosure.

The addition of L-shaped fins in Model 03 enhances heat transfer by increasing the surface area, accelerating the temperature rise, and improving the overall melting behavior. These fins facilitate better conduction at the initial stage of melting and promote natural convection as the liquid PCM forms. In Model 04, the fins are extended and thinned, further enhancing thermal performance by distributing heat more effectively throughout the PCM. The extended fins penetrate deeper into the PCM, allowing for more uniform heat dispersion and reducing the formation of unmelted regions. Model 05, with the longest and thinnest fins, achieves the most efficient heat transfer, as it maximizes the heat transfer area while maintaining optimal convective flow paths. The thinner fins minimize thermal resistance, enabling faster heat penetration, while the increased length ensures deeper heat propagation into the PCM.

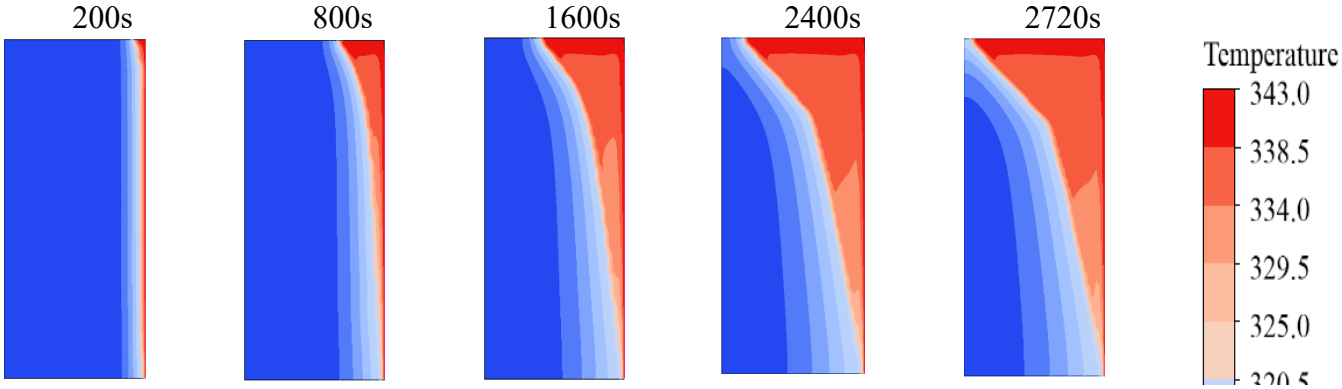

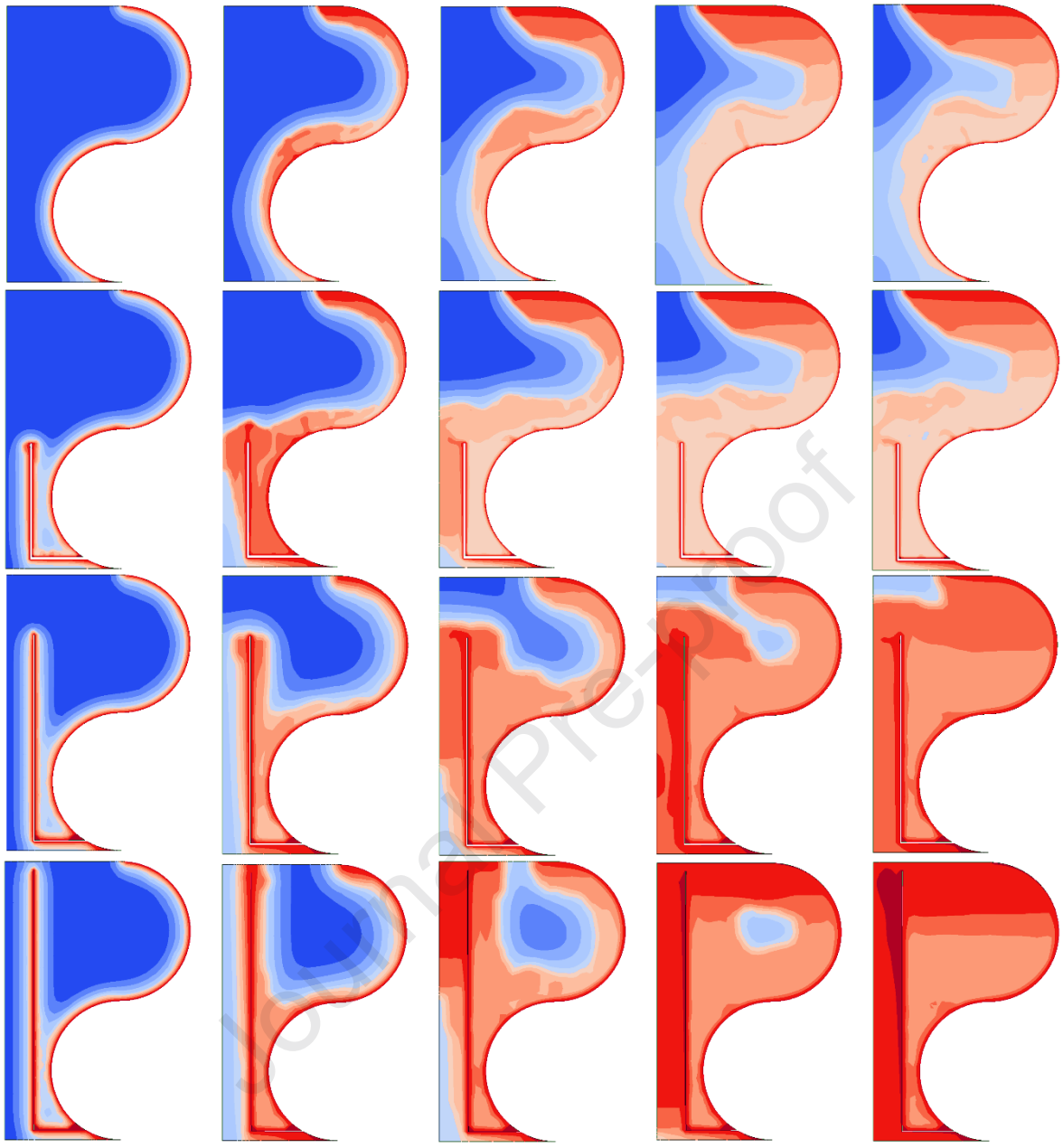

Fig 10. Comparative analysis of temperature contours for all cases in PCM-Based TES Systems.

4.1.2. Transient PCM Temperature

Figure 11 presents the average PCM temperature for all models, highlighting the differences in thermal performance. Model 05 achieves the best temperature distribution and the highest increase in PCM temperature due to the longest and thinnest fins, which maximize the heat transfer surface area and enhance natural convection, ensuring efficient heat distribution throughout the PCM. Additionally, Model 05 features an S-shaped curved profile, which increases the heat source surface and improves heat distribution.

Model 04 follows, with extended and thinner fins compared to Model 03, which improves the heat transfer process by facilitating better convection and conduction. Similar to Model 05, Model 04 also incorporates the S-shaped curved profile, contributing to its enhanced thermal performance. Model 03 exhibits improved performance due to the addition of L-shaped fins, which increase the heat transfer surface and accelerate the temperature rise. This model also benefits from the S-shaped curved profile, redistributing the PCM toward the top and increasing the heat source surface.

Model 02, with its S-shaped curved profile, increases the heat source surface and redistributes the PCM toward the top, enabling faster melting and better temperature distribution in the upper region compared to Model 01. However, it lacks the additional enhancement provided by fins. Model 01, the rectangular container, shows the lowest increase in PCM temperature due to its uniform PCM distribution, which results in slower heat transfer, particularly at the bottom of the enclosure.

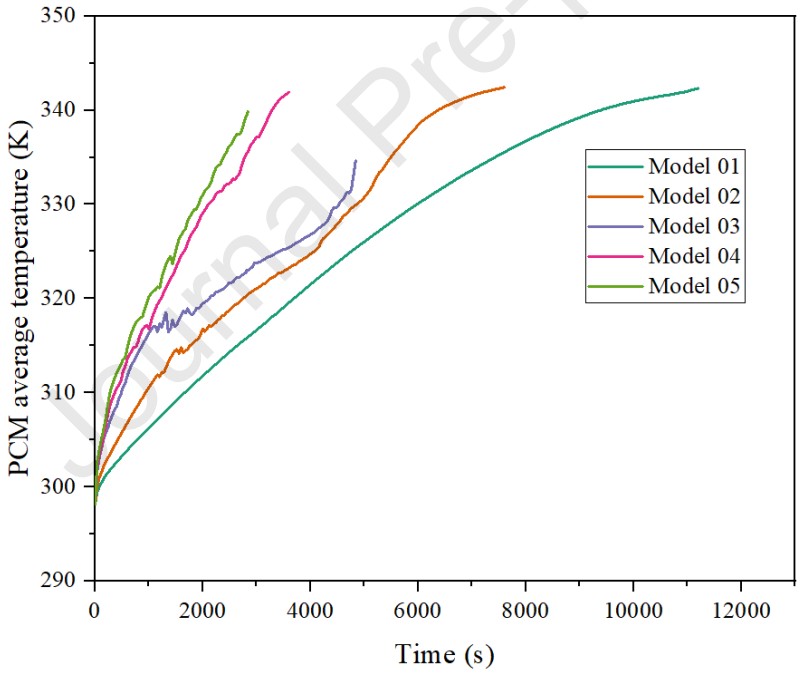

Fig 11. Temporal analysis of temperature variation in PCM-Based TES Systems.

4.2. Phase Change Behavior

4.2.1. Liquid Fraction Contours

The liquid fraction contours in **Figure 12** illustrate the evolution of the melting process for PCM in five configurations at intervals of 200s, 800s, 1600s, 2400s, and 2720s. Each model demonstrates unique melting characteristics influenced by its geometry and fin design.

In Model 01 (Rectangular container), melting begins near the heated right wall at 200s, dominated by conduction. Natural convection drives the melting upward, leaving the bottom

region with slow heat propagation. By the 800s, the melting front advances upward, but the bottom remains stagnant due to insufficient convection. Inthe 1600s, the top region exhibited more significant melting, but the bottom PCM and left sides remained largely solid. By 2400s, the PCM is still solid on the left side and left-bottom region due to the slow conduction-dominated heat transfer. At 2720s, while the top PCM is fully melted, the remaining solid PCM at the left and left bottom demonstrates an uneven and inefficient melting pattern, underscoring the need for improved heat distribution.

Model 02 (S-shaped curved profile) incorporates a curved design that redistributes PCM within the enclosure, concentrating more PCM at the top while reducing its mass at the bottom. This design modification enhances heat transfer by increasing the heated surface area, improving melting efficiency.

At 200s, melting begins near the heated wall, where the S-shaped profile facilitates a more uniform heat distribution compared to Model 01. The increased contact area between the heated wall and PCM accelerates the initial melting phase. By 800s, natural convection becomes dominant, carrying the melted, lower-density PCM upward, where a greater PCM volume is present. This results in faster melting in the upper region, while the bottom region still melts more slowly due to weaker convective currents.

Inthe 1600s, a significant portion of the PCM at the top transitioned into liquid, while the bottom showed steady but slower melting progress. The curved design aids in directing the heat flow toward the top PCM mass, improving the overall melting rate. However, by 2400s, some solid PCM remains on the left side and bottom-left region, as these areas receive less direct heat transfer.

At 2720s, the presence of residual solid PCM in these regions highlights the limitations of the S-shaped profile alone in achieving complete and uniform melting. While the design effectively accelerates melting at the top, the lower sections remain partially solid due to inefficient heat distribution. To address this, the introduction of L-shaped fins in Model 03 further enhances heat transfer, ensuring better thermal distribution across the PCM and promoting a more complete melting process.

In Model 03 (Addition of L-shaped fins), the inclusion of fins significantly enhances heat transfer by increasing the conductive surface area and improving heat distribution within the PCM. This design modification addresses the limitations of the previous models by facilitating more uniform melting throughout the enclosure.

At 200s, melting initiates around the fins, where enhanced conduction rapidly transfers heat into the surrounding PCM. A thicker molten layer forms compared to Models 01 and 02,

indicating improved heat absorption and distribution. The fins act as extended heat transfer paths, allowing heat to penetrate deeper into the PCM, reducing thermal resistance.

By the 800s, the fins play a crucial role in distributing heat evenly, accelerating melting in both the top and bottom regions. Unlike the previous models, where the bottom PCM melted at a much slower rate due to weaker convection, the fins facilitate a more balanced temperature gradient. This leads to a reduction in the melting time and minimizes the thermal stratification observed in earlier cases.

Inthe 1600s, the molten PCM extends across a significantly larger area, with the fins continuously promoting faster heat propagation. The bottom region, which previously exhibited stagnation due to slower natural convection, now shows improved melting behavior. The fins effectively channel heat toward these areas, ensuring a more uniform phase change process.

By the 2400s and 2720s, the majority of the PCM is melted, leaving only small solid fractions near the middle and left-top regions of the enclosure. These residual solid areas are significantly reduced compared to Models 01 and 02, demonstrating the effectiveness of the L-shaped fins in optimizing heat transfer and enhancing the overall thermal performance of the system.

Model 04 (Extended and thinned fins) integrates longer and thinner fins to further enhance heat transfer efficiency and enhance the melting process of the PCM. This design modification aims to maximize the heat transfer surface while maintaining efficient convective flow paths, ensuring a more uniform and rapid phase change.

At 200s, the extended fins efficiently transfer heat from the heated wall, initiating melting in a broader area compared to previous models. The elongated fins extend deeper into the PCM, allowing heat to reach regions that would otherwise remain stagnant in earlier configurations. This results in a more uniform initial melting pattern.

By the 800s, the presence of longer fins significantly improves heat distribution, ensuring simultaneous melting in the top, middle, and bottom regions. Unlike Model 03, where melting was slightly delayed in the lower regions due to weaker convective currents, Model 04 benefits from enhanced heat penetration throughout the enclosure. The thinner fins reduce thermal resistance and facilitate a more effective heat conduction process.

Inthe 1600s, a large portion of the PCM has already transitioned to liquid, with only minor solid portions remaining near the bottom and the top corners. The enhanced surface area of the fins accelerates heat absorption, reducing temperature gradients and promoting a more balanced melting progression across the enclosure.

By 2400s and 2720s, nearly all of the PCM is in a liquid state, with only small unmelted regions persisting at the top. Compared to Models 01 to 03, this configuration achieves the fastest and most uniform melting process, demonstrating the effectiveness of extended and thinned fins in improving thermal performance.

Model 05 (S-shaped profile with longest and thinnest fins) integrates the advantages of both the S-shaped enclosure and extended, thin fins, creating the most thermally efficient configuration among all models. This design maximizes the heat transfer surface while ensuring a balanced distribution of PCM, leading to a highly accelerated melting process.

At 200s, the synergy between the S-shaped profile and the longest fins promotes rapid heat penetration. The curved enclosure enhances PCM placement, ensuring that heat propagates efficiently, while the thin fins enhance conduction and facilitate an even heat distribution. This results in the fastest initial melting compared to all previous models.

By the 800s, the heat transfer enhancements lead to significant melting in both the top and bottom regions. Unlike Model 04, where some upper regions exhibited delayed melting, Model 05 ensures that both conduction and convection are utilized effectively. The S-shaped structure minimizes stagnant zones, while the elongated fins transport heat deep into the PCM.

Inthe 1600s, nearly all of the PCM has melted, with only small, isolated solid regions remaining. The curved geometry further promotes upward heat movement due to natural convection, and the fin structure ensures that heat reaches areas that would typically experience slower melting.

By 2400s, almost the entire PCM volume had transitioned to liquid, with only minor solid fractions near the middle-top region, positioned far from both the fins and the primary heat source. This small amount of remaining PCM highlights the limits of natural convection alone in achieving absolute uniformity in melting.

At 2720s, Model 05 outperforms all other configurations, achieving the most uniform and rapid melting process. The combination of an enhanced enclosure shape and highly effective fin geometry significantly enhances thermal performance, demonstrating the superior efficiency of this design in reducing melting time and maximizing heat transfer.

200s 800s 1600s 2400s 2720s

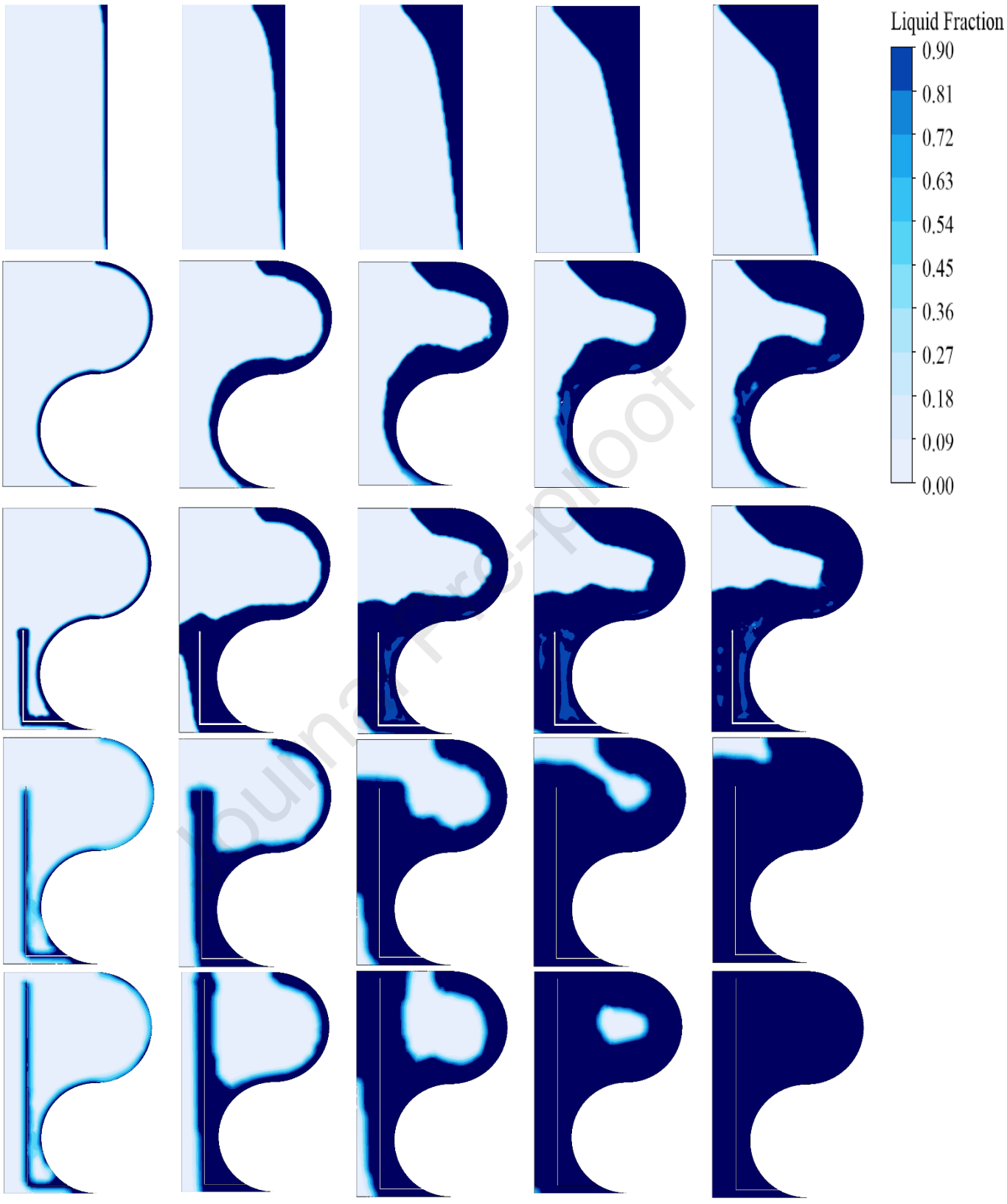

Fig 12. Comparative analysis of liquid fraction contours for all cases in PCM-Based TES Systems.

4.2.2. Transient Liquid Fraction

The melting dynamics of the five models are further analyzed through the liquid fraction curves (**Figure 13**) and the total melting time and time savings (**Figure 14**), highlighting the design modifications affecton thermal efficiency. In Model 01, the melting process is dominated by conduction, as previously observed in the liquid fraction contours. Melting begins near the heated wall, but the bottom region remains largely stagnant due to insufficient convection. This results in the slowest melting progression, with the PCM taking 11,040stothe transition to the liquid phase fully.

In Model 02, the incorporation of the S-shaped profile concentrates PCM at the top, enhancing heat transfer in that region. While the bottom region still experiences slower melting due to limited convection, the liquid fraction curve (**Figure 13**) shows an improvement over Model 01. The melting time reduces to 7,600s, achieving a 31.16% time saving, as shown in **Figure 14**.

Adding L-shaped fins in Model 03 significantly improves the melting process by increasing the conductive heat transfer surface area. The liquid fraction curve (**Figure 13**) demonstrates a more rapid progression compared to Models 01 and 02, with melting time reduced to 4,840sa56.16% time-saving (**Figure 14**).

In Model 04, the extended and thinned fins further optimize heat distribution, resulting in more uniform melting across the PCM. The liquid fraction curve (**Figure 13**) exhibits a steeper slope compared to Model 03, reflecting faster melting in all regions. This design achieves a melting time of 3,160s, corresponding to a 71.37% time saving (**Figure 14**).

Finally,Model 05 combines the S-shaped profile with the longest and thinnest fins, representing the most efficient design. The synergy between the curved profile and extended fins ensures optimal heat distribution and the fastest melting rate. The liquid fraction curve (**Figure 13**) demonstrates the steepest progression, with the PCM fully melted in just 2,720s, achieving a 75.36% time saving, as shown in **Figure 14**.

The reduction in melting time observed in Model 05 (75.36%) has important implications for applications that require rapid heat storage and release, such as industrial processes. This improvement enables more efficient thermal energy management, enhancing system responsiveness and overall performance.

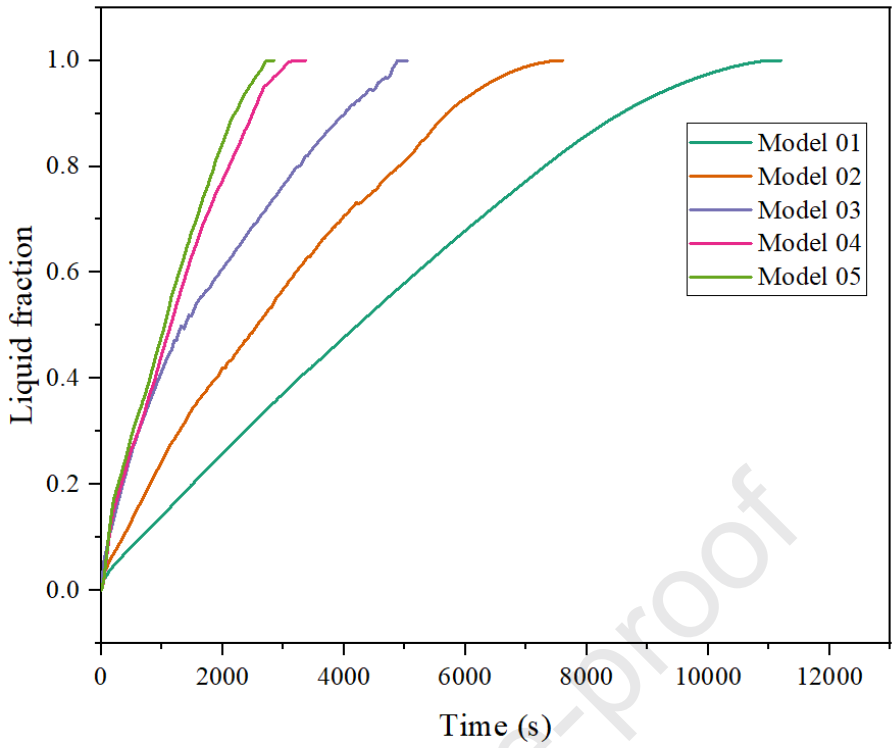

Fig 13. Temporal analysis of liquid fraction variation in PCM-Based TES Systems.

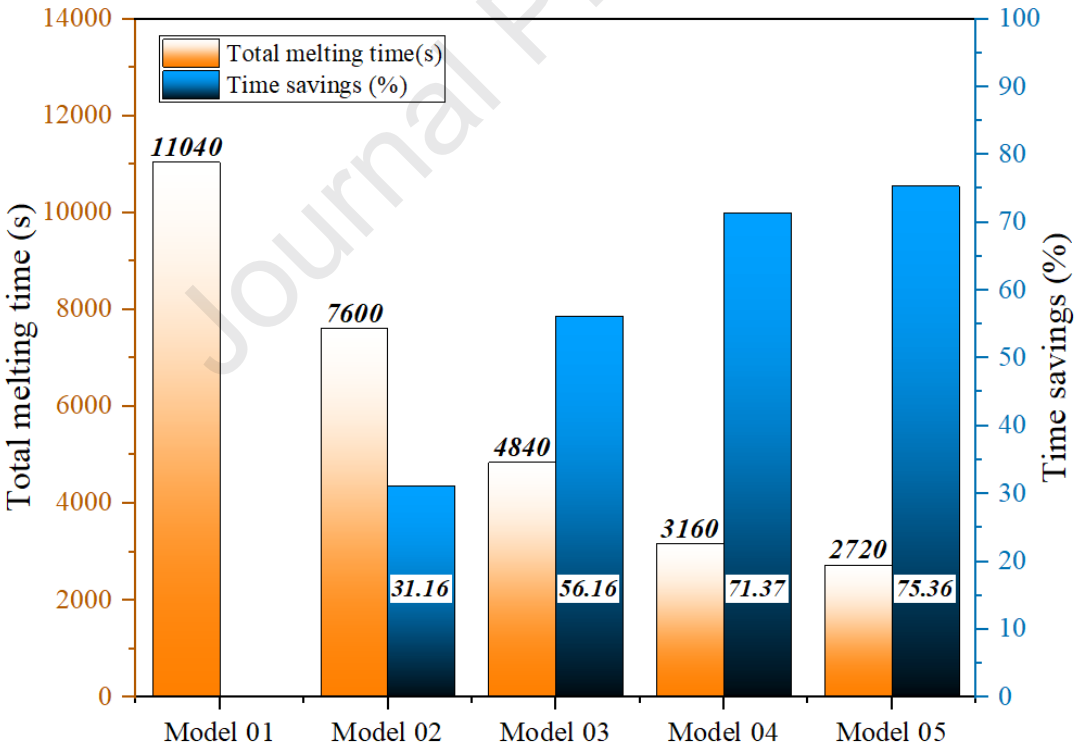

Fig 14. Comparison of melting time and time savings for different configurations.

1000s 2520s

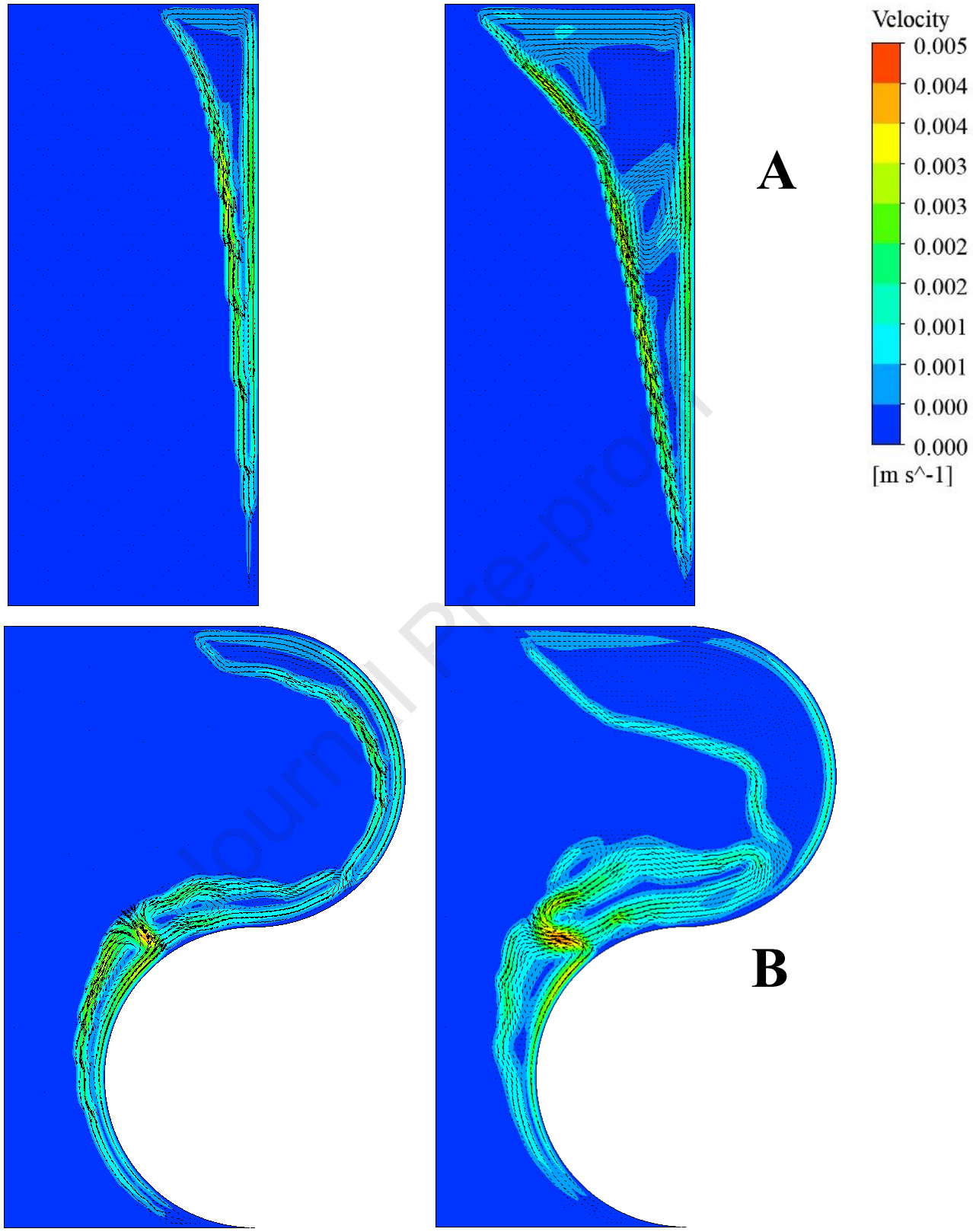

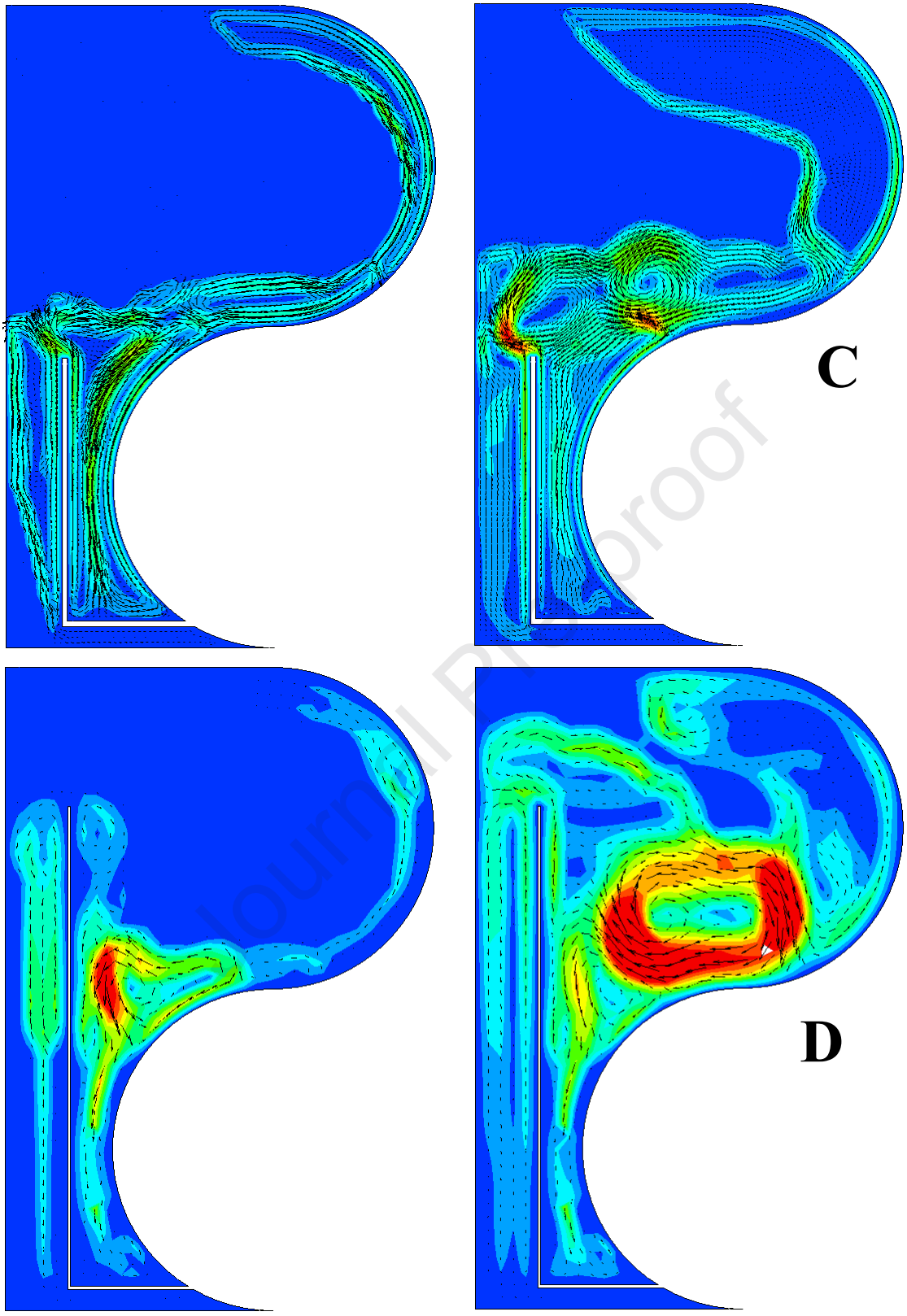

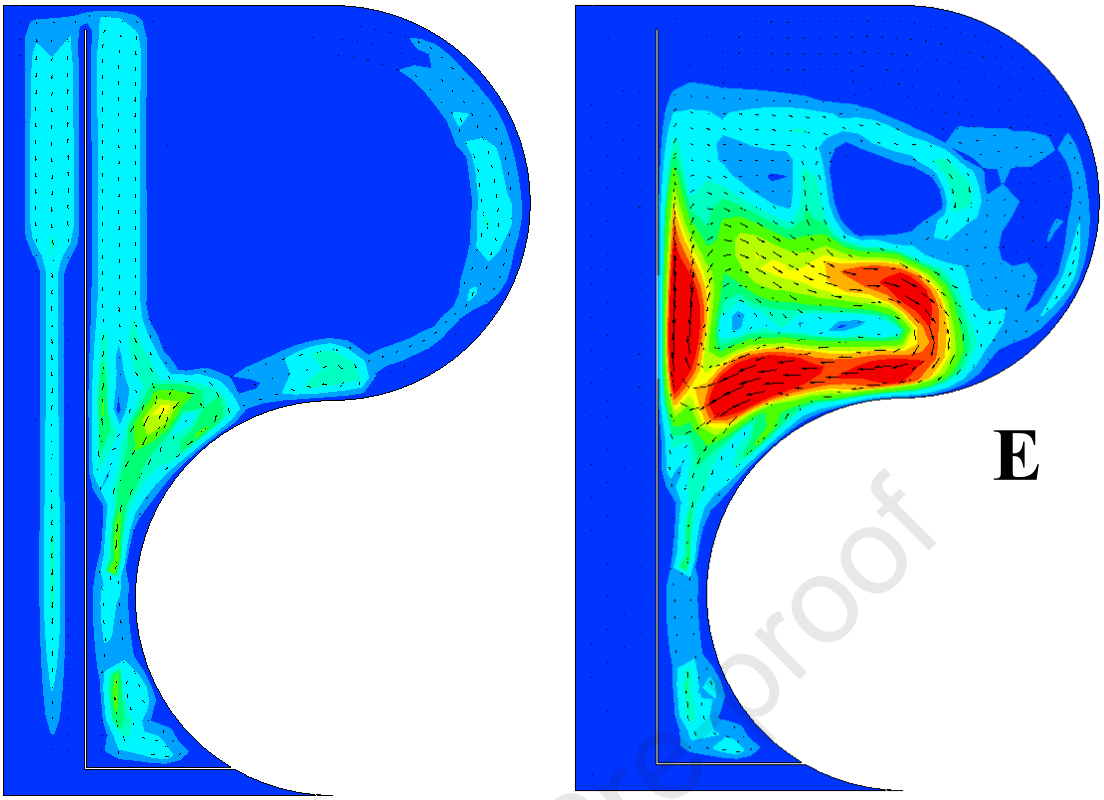

Fig 15. Velocity contours at t=1000s, and t=2520s: (A)-For Model 01, (B)-For Model 02, (C)-For Model 03, (D)-For Model04, (E)- For Model 05.

4.3. Flow Dynamics Analysis

4.3.1. Velocity Contours

Figure 15 illustrates the velocity contours at 1000s and 2520s providing insights into the flow dynamics and natural convection patterns in the PCM for each model configuration.

In Model 01 (Rectangular container), at 1000s, weak convection is observed near the heated right wall, with low-velocity magnitudes dominating the domain. By the 2520s, convection strengthened slightly in the upper region, but the bottom and left regions remained stagnant due to limited heat propagation and weak convective currents.

In Model 02 (S-shaped curved profile), at 1000s, the curved profile enhances natural convection near the top, creating higher velocity magnitudes compared to Model 01. However, the bottom region still exhibits minimal flow activity. At 2520s, the top region shows intensified convection currents, aiding in faster heat transfer, while the bottom region remains largely unaffected.

In Model 03 (Addition of L-shaped fins), at 1000s, the introduction of fins generates localized higher velocity zones near the fins and heated wall, enhancing heat transfer. By

2520s, the fins promote stronger convection currents across the enclosure, with improved flow activity in the bottom region compared to the previous models.

In Model 04 (Extended and thinned fins), at 1000s, the extended fins further enhance the velocity field, with notable improvements in flow strength and coverage across the domain. At 2520s, convection currents become more uniform, with higher velocities observed throughout the enclosure, indicating more efficient heat transfer and reduced stagnant regions.

In Model 05 (S-shaped profile with longest and thinnest fins), at 1000s, the synergy between the curved profile and extended fins generates high-velocity magnitudes across all models. By 2520s, the convection patterns are significantly enhanced, with robust flow activity throughout the enclosure, ensuring the most efficient heat transfer among all configurations.

4.3.2. Transient Velocity

Figure 16 illustrates the velocity evolution of the PCM over time for all configurations.

In Model 01, the velocity starts at a low magnitude and gradually increases over time, peaking at approximately 3.95×10^{-4} m/s at3440s. The curve demonstrates the slowest rise and overall weakest convection due to the lack of geometric features enhancing natural convection.

In Model 02, the S-shaped profile accelerates the initial rise in velocity, peaking earlier than Model 01 at a slightly higher magnitude of around 5.11×10^{-3} m/sat 2000s. However, the velocity decreases quickly due to limited flow activity in the bottom region.

In Model 03, adding fins significantly improves the peak velocity, reaching approximately 7.6×10^{-3} m/s at 2440s. The curve shows a sharper rise and sustained velocities for a longer duration compared to Models 01 and 02, highlighting the fins' contribution to enhancing convection.

In Model 04, the extended and thinned fins further optimize the velocity profile, achieving a peak of around 2×10^{-3} m/s at 2320s. The curve demonstrates the fastest rise and the most sustained high velocities, reflecting the improved heat transfer efficiency and uniform convection patterns.

In Model 05, the combination of the S-shaped profile and longest, thinnest fins results in the highest peak velocity of 1.76×10^{-3} m/s. The curve exhibits a steeper rise and more prolonged high velocities, showcasing the superior performance of this design in maximizing natural convection and reducing thermal resistance.

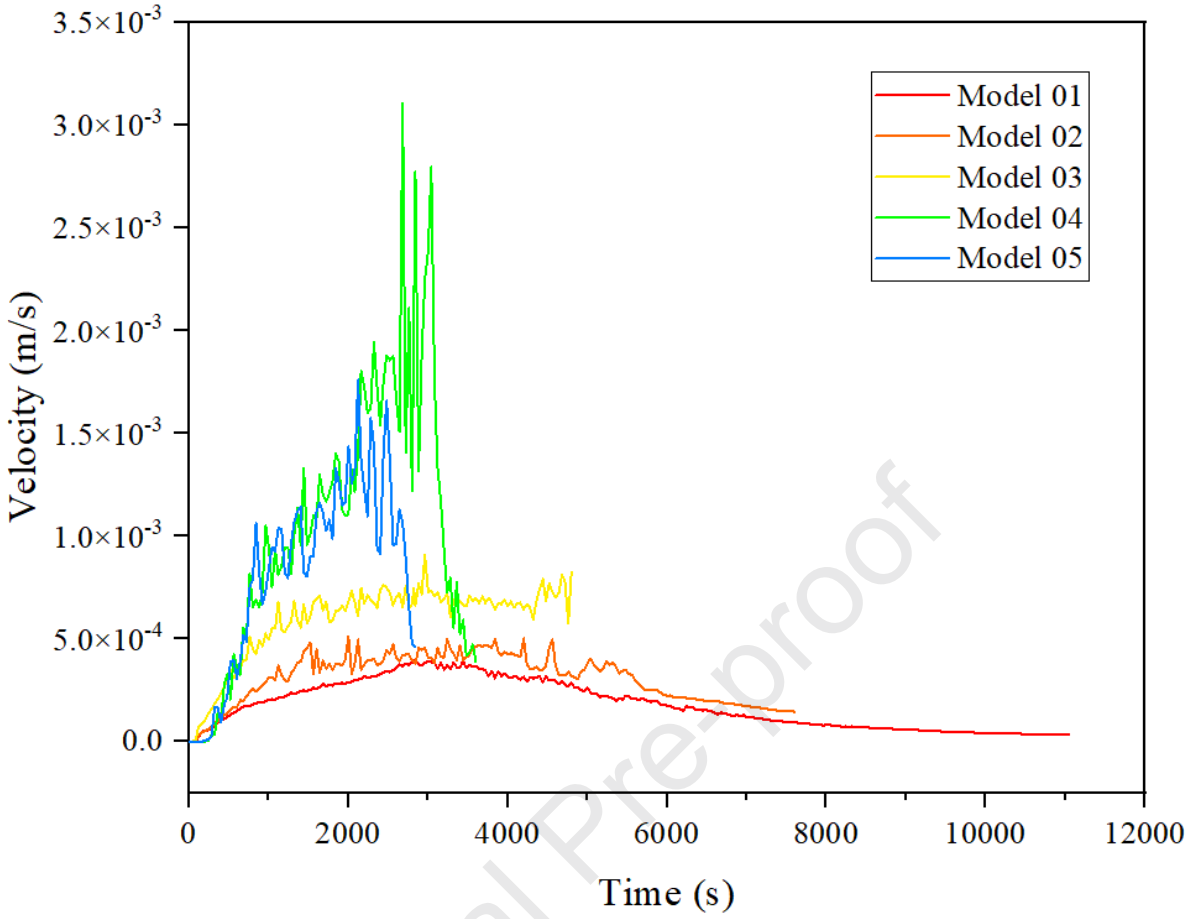

Fig 16. Velocity Variation over time for different configurations.

4.4. Heat Flux Distribution

Figure 17 illustrates the transient heat flux within the PCM enclosure for the five analyzed models throughout the melting cycle. Initially, all curves overlap, indicating that the heat flux is nearly identical across different enclosure geometries. This occurs because heat conduction dominates as the primary mode of heat transfer at the solid PCM interface. During this phase, heat is transferred through direct molecular interactions, making the geometric configuration of the enclosure less influential. As melting progresses, a liquid PCM layer forms, allowing natural convection to develop. The density gradients within the molten PCM create buoyancy-driven flows, leading to enhanced heat transfer. This effect varies across different models due to differences in enclosure geometry, which influence the strength and direction of convective currents. As a result, distinct variations in heat flux become evident. A clear trend of decreasing heat flux is observed across all models. Initially, the temperature gradient between the heat transfer surface and the PCM is high, resulting in a strong driving force for

heat transfer and, consequently, a high heat flux. However, as heat is absorbed, the temperature gradient decreases, reducing the rate of heat transfer. During the phase transition, the PCM absorbs a significant amount of latent heat, which can cause temporary stabilization or peaks in the heat flux. These variations are model-dependent, as enclosure design influences how efficiently heat is distributed within the PCM. As melting advances, a liquid PCM layer forms near the heat transfer surface, introducing thermal resistance. This layer acts as an insulator, as the convective currents may not be strong enough to counteract the reduced thermal conductivity of the liquid PCM compared to the solid phase. Once the phase change is complete, the system transitions to sensible heat transfer in the liquid phase, where heat is primarily transferred through convection rather than phase transition. This further reduces the heat flux over time. The observed differences in heat flux behavior among the five models highlight the critical role of enclosure geometry in shaping natural convection patterns and overall thermal performance.

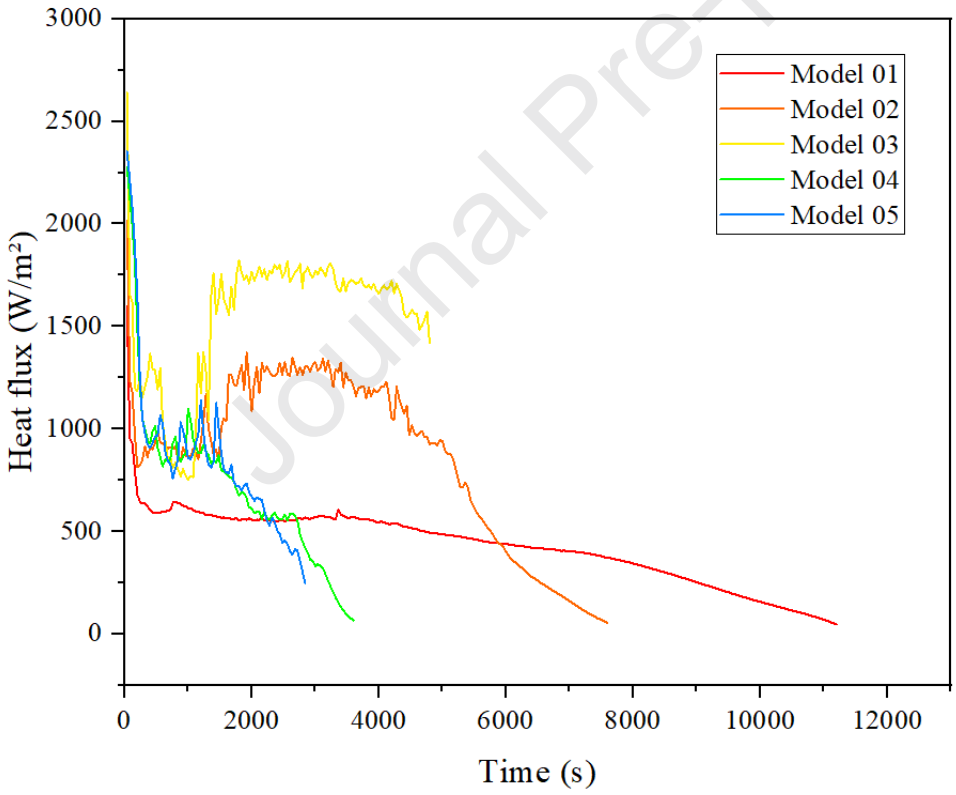

Fig 17. Variation of heat flux Over time analysis for all cases.

4.5. Thermal energy storage capacity

The energy accumulated during a phase change is known as latent heat.The stored energy of the PCM and the energy capacity of the TES system can be calculated as follows[55]:

$$Q(t) = m_{PCM}\left[\gamma\lambda + C_{P,PCM}\left(T_{ave,PCM}(t) - T_{ini}\right)\right] \quad (16)$$

Where Q(t)(KJ)is the total heat storage, m_{PCM}(kg)denotes the mass of the PCM, $T_{ave,\ PCM(t)}$(K)is the average PCM temperature at time t, $C_{p,\ PCM}$ indicates the specific heat capacity (J/kg.K)of the PCM, and T_{ini}(K) is the initial temperature.

Figure 18examines the thermal energy storage capacities for Models 01 through 05, highlighting the contributions of latent (Q_{latent}) and sensible heat ($Q_{sensible}$). Across the models, variations in total energy storage capacity are influenced by differences in PCM mass and design features. Model 01 achieves a total energy storage capacity of 191.5 kJ, with 126.7 kJ from latent heat and 64.8 kJ from sensible heat. This high latent heat contribution is due to the longer melting time (11040 seconds). In Model 02, the total energy storage increases slightly to 192.04 kJ, with 126.7 kJ from latent heat and 65.34 kJ from sensible heat. This enhancement is attributed to the S-shaped profile, which enhances heat transfer and effectively distributes heat toward the PCM. Model 03 shows the lowest total energy storage of 178.85 kJ, comprising 125.05 kJ from latent heat and 53.8 kJ from sensible heat. This reduction is due to the fins with the largest thickness (1 mm), which occupy more volume, thereby reducing the PCM mass and its latent heat storage capacity. Model 04 achieves a total energy storage of 184.91 kJ, with 125.43 kJ from latent heat and 59.48 kJ from sensible heat. This model's thinner (0.5 mm) and longer fins allow for more PCM mass while maintaining efficient heat transfer. Similarly, Model 05 records a total energy storage of 184.2 kJ, with 125.8 kJ from latent heat and 58.4 kJ from sensible heat, performing comparably to Model 04 due to similar fin thickness (0.3 mm) and length (112.3 mm).

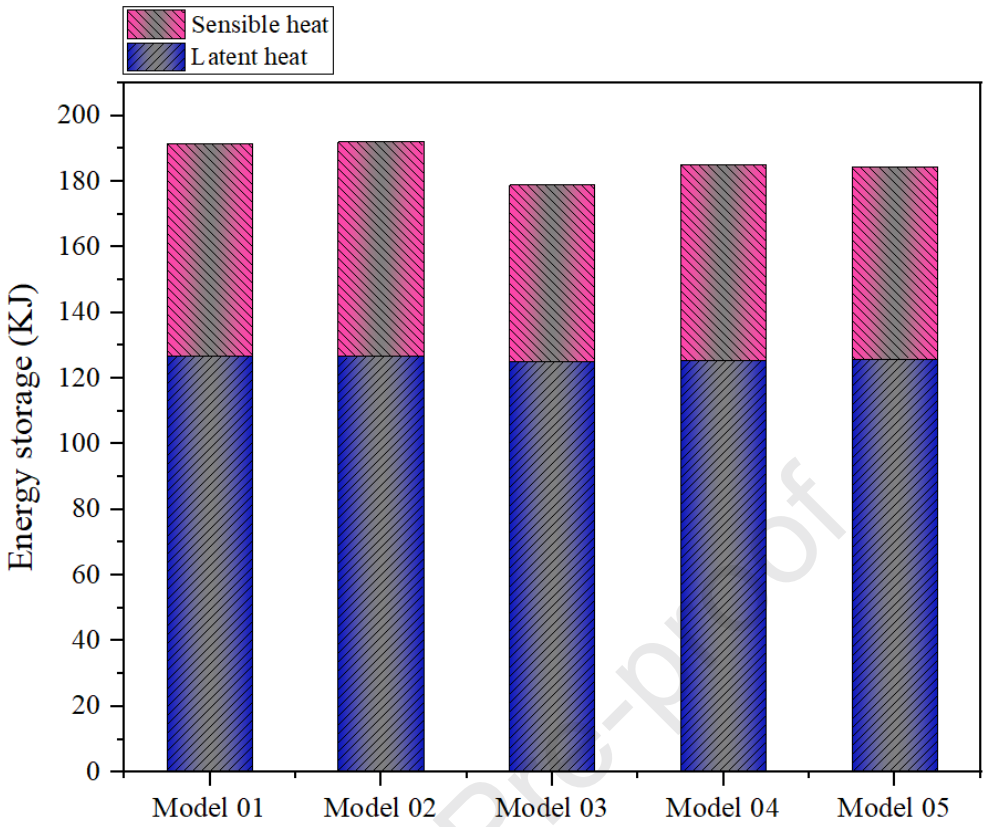

Fig 18. Evaluation of TES capacities analysis of efficiency and performance for all cases.

4.6. Energy storage density and mean power

To assess the PCM's energy storage performance, the parameter SE_m, referred to as energy storage density[56], is defined as the ratio of the PCM's stored energy to its mass (m_{PCM}), as expressed in Eq. (17).

$$SE_m = Q(t) \Big/ m_{PCM} \tag{17}$$

Here, Q(t)represents the PCM's stored energy, which can be determined using Eq. (16) provided above.

Figure 19 illustrates the energy storage density $SE_m$and mean power P_m for different models during the melting process. Model 01 achieves the highest SE_m of **282.96 kJ/kg** due to its long melting time of **11,040 s**, allowing for prolonged heat absorption. In contrast, Model 02 demonstrates an even higher SE_m of **283.76 kJ/kg**, with a shorter melting time of **7,600 s,**attributed to the S-shaped enclosure, which enhances heat transfer through natural convection, concentrating heat at the top of the enclosure where the PCM absorbs it more effectively. Model 03 exhibits the lowest SE_m of **267.74 kJ/kg**, as the thicker fins (1 mm) reduce PCM mass and storage capacity, despite completing the melting process in **4,840 s.** Model 04, with thinner fins (0.5 mm), achieves a higher SE_m of **275.99 kJ/kg** and completes melting in **3,160 s**, striking a balance between PCM mass and efficient heat transfer. Similarly, Model 05 achieves a $SE_m$of *274.12* **kJ/kg** and completes melting in just **2,720 s**, benefiting from thin fins (0.3) that enhance heat absorption and storage within the shortest time.

The mean power, P_m, is defined as the ratio of the PCM's stored energy to its total melting time(t_{PCM}), as expressed in Eq. (18).

$$P_m = Q(t) \Big/ t_{PCM} \tag{18}$$

Figure 19 also highlights the trend in mean power P_m across the models, which increases progressively from Model 01 to Model 05 as the melting time decreases. Model 01, with the longest melting time of 11,040 s, has the lowest $P_m$of 17.34 W. In contrast, Model 02, with a shorter melting time of 7,600 s, achieves a higher $P_m$of 25.26 W, benefiting from the enhanced heat transfer provided by the S-shaped enclosure. Model 03, having a reduced melting time of 4,840 s, exhibits a good P_m of 36.95 W. Model 04 achieves a P_m of 58.51 W, supported by its fins and a faster melting time of 3,160 s. Finally, Model 05 demonstrates the highest $P_m$of 67.72 W, attributed to its longer fins, efficient heat transfer, and shortest melting time of 2,720 s. This consistent increase in P_m reflects the improved energy absorption rates and faster heat transfer as the melting time decreases across the models.

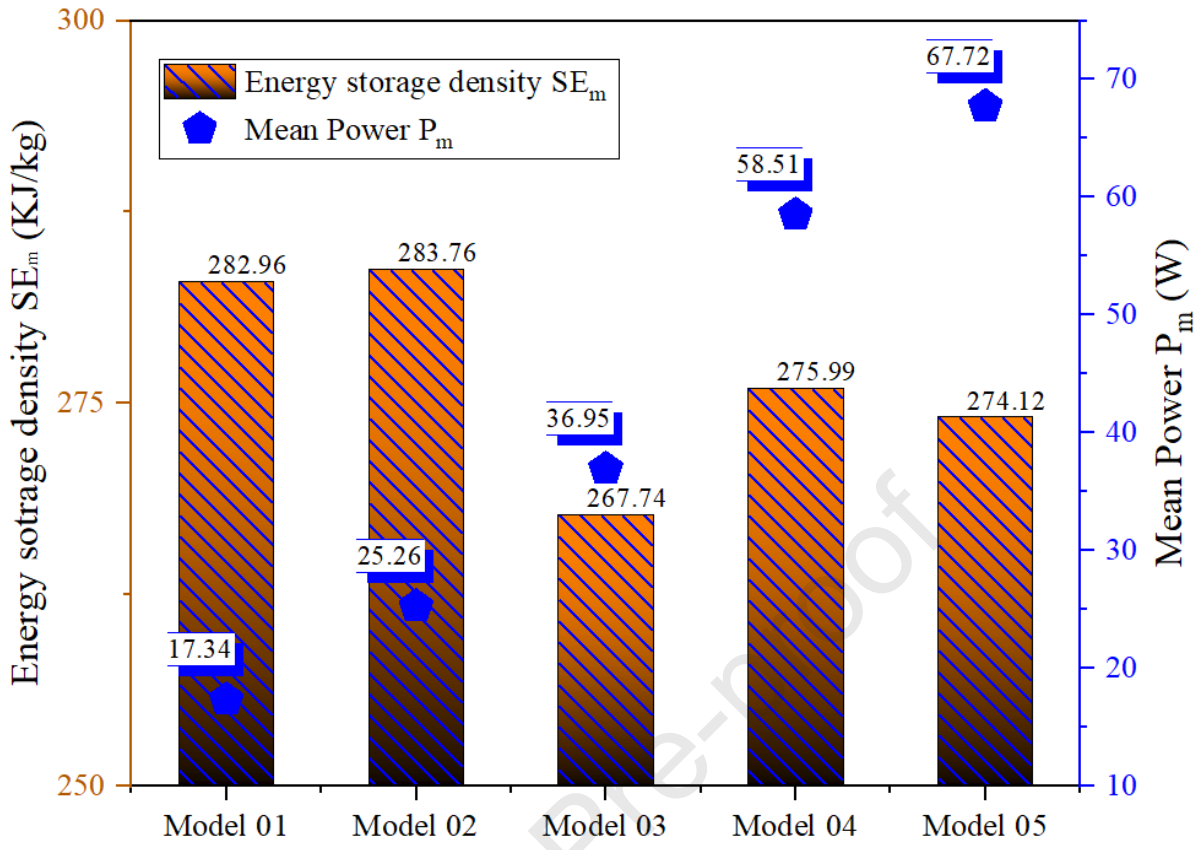

Fig 19. Energy storage density and mean power across all Models.

5. Conclusion

This study investigates the enhancement of TES systems by analyzing the influence of geometric modifications, including L-shaped fins and an S-shaped heat source wall, on phase change behavior and heat transfer performance. The numerical results demonstrate that these design enhancements significantly improve melting efficiency, energy storage capacity, and overall system performance.Key findings of the study include:

- The enhanced designs led to a substantial reduction in melting time. Compared to Model 01, Model 02 achieved a 31.16% reduction, Model 03 reduced melting time by 56.16%, Model 04 by 71.37%, and Model 05 by 75.36%, demonstrating the effectiveness of fins and the S-shaped heat source wall in accelerating phase change.

- The highest SE_m of 274.12 kJ/kg was observed in Model 05, highlighting the role of geometric modifications in enhancing heat storage capacity.

- The P_m was also maximized in Model 05, reaching 67.72 W, further emphasizing the advantages of the enhanced fin and wall configurations.

- The incorporation of thinner (0.3 mm) and longer (112.3 mm) fins, coupled with the S-shaped heat source wall, proved to be the most effective strategy for improving heat transfer and storage efficiency, achieving the highest total heat storage capacity of 184.2 kJ.

These findings underscore the importance of advanced geometric enhancement in TES design. The integration of enhanced fin geometries and enclosure profiles provides a promising approach for developing more efficient TES systems, with potential applications in renewable energy storage and thermal management.

Acknowledgment

The authors extend their appreciation to Taif University, Saudi Arabia, for supporting this work through project number (TU-DSPP-2024-145). Additionally, Dr. Nahid Fatima would like to thanks Prince Sultan University Riyadh for support and help through TAS lab.

Funding

This research was funded by Taif University, Saudi Arabia, project No. (TU-DSPP-2024-145).

References

[1] L. Ahmad, N. Khordehgah, J. Malinauskaite, and H. Jouhara, "Recent advances and applications of solar photovoltaics and thermal technologies," *Energy*, vol. 207, p. 118254, 2020, doi: 10.1016/j.energy.2020.118254.

[2] E. Loth, C. Qin, J. G. Simpson, and K. Dykes, "Why we must move beyond LCOE for renewable energy design, Advances in Applied Energy, 8, 100112." 2022.

[3] J. Mitra and N. Nguyen, "Grid-scale virtual energy storage to advance renewable energy penetration," *IEEE Trans. Ind. Appl.*, vol. 58, no. 6, pp. 7952–7965, 2022.

[4] C. Liu, F. Li, L. Ma, and H. Cheng, "Advanced materials for energy storage," *Adv. Mater.*, vol. 22, no. 8, pp. E28–E62, 2010.

[5] P. D. Tagle-Salazar, K. D. P. Nigam, and C. I. Rivera-Solorio, "Parabolic trough solar collectors: A general overview of technology, industrial applications, energy market, modeling, and standards," *Green Process. Synth.*, vol. 9, no. 1, pp. 595–649, 2020.

[6] M. S. El-Sebaey, S. M. T. Mousavi, R. Sathyamurthy, H. Panchal, and F. A. Essa, "A detailed review of various design and operating parameters affecting the thermal performance augmentation of flat-plate solar collectors," *Int. J. Ambient Energy*, vol. 45, no. 1, p. 2351100, 2024.

[7] C. Prieto, F. J. Ruiz-Cabanas, V. Madina, A. I. Fernández, and L. F. Cabeza, "Corrosion performance of alloy 800H and alloy 625 for potential use as molten salts solar receiver materials in concentrating solar power tower plants," *J. Energy Storage*, vol. 55, p. 105824, 2022.

[8] F. Hassan *et al.*, "Recent advancements in latent heat phase change materials and their applications for thermal energy storage and buildings: A state of the art review," *Sustain. Energy Technol. Assessments*, vol. 49, no. November 2021, p. 101646, 2022, doi: 10.1016/j.seta.2021.101646.

[9] Z. Khan, Z. Khan, and A. Ghafoor, "A review of performance enhancement of PCM based latent heat storage system within the context of materials, thermal stability and compatibility," *Energy Convers. Manag.*, vol. 115, pp. 132–158, 2016.

[10] M. K. Rathod and J. Banerjee, "Thermal stability of phase change materials used in latent heat energy storage systems: A review," *Renew. Sustain. energy Rev.*, vol. 18, pp. 246–258, 2013.

[11] S. A. Tat and P. Muthukumar, "Experimental study on the thermal performance of a high-temperature finned latent heat storage system," *Renew. Energy*, vol. 235, p. 121315, 2024.

[12] H. E. Abdellatif, A. Belaadi, H. Alshahrani, M. K. A. Khan, and M. Bourchak, "Modeling three-dimensional flow in a thermal energy tank: Numerical analysis of the impact of tank shape on the melting and solidification of phase change material," *J. Energy Storage*, vol. 72, no. April, p. 108286, 2023, doi: 10.1016/j.est.2023.108286.

[13] H. E. Abdellatif, A. Belaadi, A. Arshad, M. Bourchak, and D. Ghernaout, "Enhanced solar energy utilization of thermal energy storage tanks with phase change material and baffle incorporating holes," *Therm. Sci. Eng. Prog.*, vol. 52, no. November, pp. 2022–2023, 2024, doi: 10.1016/j.tsep.2024.102674.

[14] G. Alva, Y. Lin, and G. Fang, "An overview of thermal energy storage systems," *Energy*, vol. 144, pp. 341–378, 2018.

[15] A. Sharma, V. V. Tyagi, C. R. Chen, and D. Buddhi, "Review on thermal energy storage with phase change materials and applications," *Renew. Sustain. Energy Rev.*, vol. 13, no. 2, pp. 318–345, 2009, doi: 10.1016/j.rser.2007.10.005.

[16] I. Sarbu and C. Sebarchievici, "A comprehensive review of thermal energy storage," *Sustainability*, vol. 10, no. 1, p. 191, 2018.

[17] N. Ben Khedher *et al.*, "Geometry modification of a vertical shell-and-tube latent heat thermal energy storage system using a framed structure with different undulated

shapes for the phase change material container during the melting process," *J. Energy Storage*, vol. 72, no. PB, p. 108365, 2023, doi: 10.1016/j.est.2023.108365.

[18] N. Ben Khedher *et al.*, "Discharge performance assessment of a vertical double-pipe latent heat storage unit equipped with circular Y-shaped fins," *J. Build. Eng.*, vol. 75, no. March, p. 106870, 2023, doi: 10.1016/j.jobe.2023.106870.

[19] P. T. Sardari, H. I. Mohammed, D. Giddings, G. S. walker, M. Gillott, and D. Grant, "Numerical study of a multiple-segment metal foam-PCM latent heat storage unit: Effect of porosity, pore density and location of heat source," *Energy*, vol. 189, p. 116108, 2019, doi: https://doi.org/10.1016/j.energy.2019.116108.

[20] W. B. Ye and M. Arıcı, "False diffusion, asymmetrical interface, and equilibrious state for pure solid-gallium phase change modeling by enthalpy-porosity methodology," *Int. Commun. Heat Mass Transf.*, vol. 144, p. 106746, 2023, doi: 10.1016/j.icheatmasstransfer.2023.106746.

[21] J. Jeon, J.-H. Lee, J. Seo, S.-G. Jeong, and S. Kim, "Application of PCM thermal energy storage system to reduce building energy consumption," *J. Therm. Anal. Calorim.*, vol. 111, pp. 279–288, 2013.

[22] Y. Liu, Y. Sun, D. Gao, J. Tan, and Y. Chen, "Stacked ensemble learning approach for PCM-based double-pipe latent heat thermal energy storage prediction towards flexible building energy," *Energy*, vol. 294, p. 130955, 2024.

[23] T. A. Mukram and J. Daniel, "Performance evaluation of a novel cement brick filled with micro-PCM used as a thermal energy storage system in building walls," *J. Energy Storage*, vol. 77, p. 109910, 2024.

[24] N. Soares, A. R. Gaspar, P. Santos, and J. J. Costa, "Experimental evaluation of the heat transfer through small PCM-based thermal energy storage units for building applications," *Energy Build.*, vol. 116, pp. 18–34, 2016, doi: 10.1016/j.enbuild.2016.01.003.

[25] H. E. Abdellatif, A. Belaadi, H. Alshahrani, and M. K. A. Khan, "Efficiency enhancement in solar energy storage: Impact of oval inner tube geometries on phase change material units," *Numer. Heat Transf. Part A Appl.*, vol. 0, no. 0, pp. 1–28, 2024, doi: 10.1080/10407782.2024.2332478.

[26] S. Ali, H. Eddine, A. Belaadi, A. Arshad, and H. Liu, "Numerical study of shell and tube thermal energy storage system : Enhancing solidification performance with single-walled carbon nanotubes in phase change material," *Int. Commun. Heat Mass Transf.*, vol. 160, p. 108338, 2025, doi: 10.1016/j.icheatmasstransfer.2024.108338.

[27] G. Gholamibozanjani and M. Farid, “Application of an active PCM storage system into a building for heating/cooling load reduction,” in *Thermal Energy Storage with Phase Change Materials*, CRC Press, 2021, pp. 331–358.

[28] S. Lee, H. Choi, P. Park, S. Kang, K. Choi, and H. Lee, “Investigation of enhanced PCM heat sink design under extreme thermal conditions for high-heat-generating electronic devices,” *Int. Commun. Heat Mass Transf.*, vol. 159, p. 108050, 2024.

[29] R. Balakrishnan, K. Govindaraj, A. Mahalingam, and Y. Devarajan, “Analysis of the thermal management of electronic equipment by employing silicon carbide nano-pcm-based heat sink,” *Environ. Sci. Pollut. Res.*, vol. 31, no. 34, pp. 46376–46384, 2024.

[30] V. V Tyagi *et al.*, “Sustainable growth of solar drying technologies: Advancing the use of thermal energy storage for domestic and industrial applications,” *J. Energy Storage*, vol. 99, p. 113320, 2024.

[31] S. P. Patel and M. K. Rathod, “Improving Wastewater Heat Recovery Using Phase Change Material Heat Exchangers: A Numerical Study of Thermal Performance,” *Energy Storage*, vol. 6, no. 6, p. e70018, 2024.

[32] M. A. Yedmel, R. Hunlede, S. Lacour, G. Alvarez, A. Delahaye, and D. Leducq, “A novel approach combining thermosiphon and phase change materials (PCM) for cold energy storage in cooling systems: A proof of concept,” *Int. J. Refrig.*, vol. 158, pp. 393–404, 2024.

[33] S. K. Sahoo, M. K. Das, and P. Rath, “Application of TCE-PCM based heat sinks for cooling of electronic components: A review,” *Renew. Sustain. Energy Rev.*, vol. 59, pp. 550–582, 2016.

[34] S. F. Hosseinizadeh, F. L. Tan, and S. M. Moosania, “Experimental and numerical studies on performance of PCM-based heat sink with different configurations of internal fins,” *Appl. Therm. Eng.*, vol. 31, no. 17–18, pp. 3827–3838, 2011.

[35] H. M. Sadeghi, M. Babayan, and A. Chamkha, “Investigation of using multi-layer PCMs in the tubular heat exchanger with periodic heat transfer boundary condition,” *Int. J. Heat Mass Transf.*, vol. 147, no. xxxx, 2020, doi: 10.1016/j.ijheatmasstransfer.2019.118970.

[36] N. S. Dhaidan, A. F. Hassan, A. M. Rasheed Al-Gaheeshi, F. N. Al-Mousawi, and R. Z. Homod, “Experimental investigation of thermal characteristics of phase change material in finned heat exchangers,” *J. Energy Storage*, vol. 71, no. June, 2023, doi: 10.1016/j.est.2023.108162.

[37] A. M. Abed *et al.*, “Numerical analysis of the energy-storage performance of a PCM-

based triplex-tube containment system equipped with arc-shaped fins," *Front. Chem.*, vol. 10, no. December, pp. 1–18, 2022, doi: 10.3389/fchem.2022.1057196.

[38] N. S. Dhaidan and J. M. Khodadadi, "Melting and convection of phase change materials in different shape containers: A review," *Renew. Sustain. Energy Rev.*, vol. 43, pp. 449–477, 2015, doi: 10.1016/j.rser.2014.11.017.

[39] F. Selimefendigil and H. F. Öztop, "Mixed convection in a PCM filled cavity under the influence of a rotating cylinder," *Sol. Energy*, vol. 200, pp. 61–75, 2020.

[40] A. El Khadraoui, S. Bouadila, S. Kooli, A. Guizani, and A. Farhat, "Solar air heater with phase change material: An energy analysis and a comparative study," *Appl. Therm. Eng.*, vol. 107, pp. 1057–1064, 2016, doi: 10.1016/j.applthermaleng.2016.07.004.

[41] M. Palacio, C. Ramírez, M. Carmona, and C. Cortés, "Effect of phase-change materials in the performance of a solar air heater," *Sol. Energy*, vol. 247, pp. 385–396, 2022.

[42] B. Brahma, A. K. Shukla, and D. C. Baruah, "Design and performance analysis of solar air heater with phase change materials," *J. Energy Storage*, vol. 61, p. 106809, 2023.

[43] P. Balakrishnan, S. K. Vishnu, J. Muthukumaran, and R. Senthil, "Experimental thermal performance of a solar air heater with rectangular fins and phase change material," *J. Energy Storage*, vol. 84, p. 110781, 2024.

[44] P. Rawat and A. F. Sherwani, "Optimization of single and double pass solar air heater-phase change material (SAH-PCM) system based on thickness to length ratio," *Int. J. Heat Mass Transf.*, vol. 224, p. 125356, 2024.

[45] M. K. El-Fakharany, A.-E. A. Abo-Samra, A. M. Abdelmaqsoud, and S. A. Marzouk, "Enhanced performance assessment of an integrated evacuated tube and flat plate collector solar air heater with thermal storage material," *Appl. Therm. Eng.*, vol. 243, p. 122653, 2024.

[46] M. Fadl and P. C. Eames, "Numerical investigation of the influence of mushy zone parameter Amush on heat transfer characteristics in vertically and horizontally oriented thermal energy storage systems," *Appl. Therm. Eng.*, vol. 151, no. June 2018, pp. 90–99, 2019, doi: 10.1016/j.applthermaleng.2019.01.102.

[47] W. B. Ye and M. Arıcı, "3D validation, 2D feasibility, corrected and developed correlations for pure solid-gallium phase change modeling by enthalpy-porosity methodology," *Int. Commun. Heat Mass Transf.*, vol. 144, p. 106780, 2023, doi:

10.1016/j.icheatmasstransfer.2023.106780.

[48] A. V. Arasu and A. S. Mujumdar, “Numerical study on melting of paraffin wax with Al 2O 3 in a square enclosure,” *Int. Commun. Heat Mass Transf.*, vol. 39, no. 1, pp. 8–16, 2012, doi: 10.1016/j.icheatmasstransfer.2011.09.013.

[49] H. E. Abdellatif, A. Belaadi, A. Arshad, B. X. Chai, and D. Ghernaout, “Enhancing thermal energy storage system efficiency : Geometric analysis of phase change material integrated wedge-shaped heat exchangers,” *Appl. Therm. Eng.*, p. 125268, 2024, doi: 10.1016/j.applthermaleng.2024.125268.

[50] H. Eddine, S. Ali, A. Belaadi, and D. Ghernaout, “Enhancing thermal energy storage : The impact of inclined enclosure geometry and artificial neural network based modeling on phase change material melting performance,” *J. Energy Storage*, vol. 114, no. PA, p. 115750, 2025, doi: 10.1016/j.est.2025.115750.

[51] X. Huang, F. Li, L. Lu, Z. Li, X. Yang, and J. Yan, “Depth optimization of solidification properties of a latent heat energy storage unit under constant rotation mechanism,” *Energy Build.*, vol. 290, no. April, 2023, doi: 10.1016/j.enbuild.2023.113099.

[52] W. B. Ye and M. Arıcı, “Redefined interface error, 2D verification and validation for pure solid-gallium phase change modeling by enthalpy-porosity methodology,” *Int. Commun. Heat Mass Transf.*, vol. 147, p. 106952, 2023, doi: 10.1016/j.icheatmasstransfer.2023.106952.

[53] B. Kamkari, H. Shokouhmand, and F. Bruno, “Experimental investigation of the effect of inclination angle on convection-driven melting of phase change material in a rectangular enclosure,” *Int. J. Heat Mass Transf.*, vol. 72, pp. 186–200, 2014, doi: 10.1016/j.ijheatmasstransfer.2014.01.014.

[54] W. B. Ye and M. Arıcı, “Exploring mushy zone constant in enthalpy-porosity methodology for accurate modeling convection-diffusion solid-liquid phase change of calcium chloride hexahydrate,” *Int. Commun. Heat Mass Transf.*, vol. 152, p. 107294, 2024, doi: 10.1016/j.icheatmasstransfer.2024.107294.

[55] K. S. Reddy, V. Mudgal, and T. K. Mallick, “Review of latent heat thermal energy storage for improved material stability and effective load management,” *J. Energy Storage*, vol. 15, pp. 205–227, 2018, doi: 10.1016/j.est.2017.11.005.

[56] J. Jiang, Y. Hong, Q. Li, and J. Du, “Numerical analysis on heat transfer and melting characteristics of a solid-liquid phase change process in a rectangular cavity inserted with bifurcated fractal fins,” *Int. Commun. Heat Mass Transf.*, vol. 142, no. January, p.

106616, 2023, doi: 10.1016/j.icheatmasstransfer.2023.106616.

The authors declared that they have no conflict of interest and the paper presents their own work which does not been infringe any third-party rights, especially authorship of any part of the article is an original contribution, not published before and not being under consideration for publication elsewhere.